TECHNISCHE
UNIVERSITÄT
WIEN

Master Thesis

Localization with Vehicular WLAN based on Null Frame Round Trip Time Measurement

A Thesis Submitted in Partial Fulfillment of the Requirements for the Degree of

MASTER OF SCIENCE

under the supervision of

Univ.-Prof. Dipl.-Ing. Dr.-Ing. Christoph F. Mecklenbräuker
Institute of Telecommunications

by

Richard Pfister
Mat.-Nr. 01225682

Vienna, November 2020

Abstract

A significant part of Intelligent Transport Systems (ITS) is the precise location determination of users in the transport network. Global Navigation Satellite Systems (GNSS) are commonly used, but they are likely to suffer from persistent outages when driving through tunnels. Impairment of the propagation path between satellite and receiver due to interference with other RF signals or blockage due to shadowing will also corrupt the performance. In this thesis, an easy to deploy, low-cost localization application for existing roadside units (RSU) is presented. The goal is to augment the position estimation obtained from a GNS system. The proposed approach is set up on the acknowledgment procedure of IEEE 802.11 based systems, which are commonly used in ITS. Here, a data packet is positively acknowledged with an acknowledgment (ack) frame. The round trip time (RTT) between sending a frame and receiving the acknowledgment frame can be exploited to calculate a pseudorange. Using two spatially separated RSUs, and trilateration of the RTT readings, an 802.11 device can be localized. Before starting with the implementation, the used radio module was extensively tested to identify possible dependencies regarding among others, the reliance on temperature, modulation and rate, a correlation between the RTT and transmit power, and the effect of multipath propagation. In the following, MATLAB was used to simulate the application before implementing it into C code. Subsequently, the ITS-G5 protocol stack, which is deployed on the RSUs, was modified to extract the RTT readings that are further processed in an evaluation unit. Hereby, care was taken to keep the impact of the localization application as small as possible since the main functionality should not be disturbed. The implementation was tested outdoors in three measurement campaigns. While doing so, different RSU positions, antenna setups, and transmission parameters were used. After each measurement series, the implementation was further improved. It showed that multipath propagation has a significant influence, whereby an accurate and robust estimation is only possible in a virtually ideal environment, making it impractical for the use in real-world conditions. However, combining the presented method with received signal strength measurements and using an additional RSU could substantially improve the estimation accuracy.

Zusammenfassung

Ein wesentlicher Teil in Intelligenten Verkehrssystemen (IVS) ist die genaue Standortbestimmung der Nutzer im Verkehrsnetz. Üblicherweise wird dazu ein Globales Navigationssatellitensystem (GNSS) verwendet. Dabei kann es aber zu anhaltenden Ausfällen kommen, wenn der Teilnehmer z.B.: durch einen Tunnel fährt. Störungen können unter anderem auch auftreten, wenn es im Ausbreitungsweg zwischen Satelliten und Empfänger zu Beeinträchtigungen durch Interferenzen mit anderen HF-Signalen oder zu einer Blockade durch Abschattung, kommt. In dieser Arbeit wird eine einfach zu implementierende, kostengünstige Lokalisierungsanwendung für bestehende Road Side Units (RSU) präsentiert. Ziel ist es, die von einem GNS-System erhaltene Positionsschätzung zu verbessern. Der vorgeschlagene Ansatz basiert auf der in IEEE 802.11 Netzwerken verwendeten Acknowledgement (Ack) Prozedur. Hierbei wird der Erhalt eines Datenpakets mit einem Acknowledgement Frame bestätigt. Anhand der Paketumlaufzeit bzw. Round Trip Time (RTT) zwischen dem Senden eines Datenpakets und dem Empfang des Ack Frames, kann die Distanz zwischen Sender und Empfänger ermittelt werden. Mittels zwei unterschiedlich positionierten RSUs und Trilateration der RTT-Messwerte ist es möglich ein IEEE 802.11 fähiges Gerät zu lokalisieren. Vorab wurde das verwendete Funkmodul ausgiebig getestet, um mögliche Einflussfaktoren zu identifizieren. Dabei wurde u.a. die Abhängigkeit von Temperatur, von Modulation und Informationsrate, sowie Korrelation zwischen RTT und Sendeleistung und dem Einfluss von Mehrwegeausbreitung ermittelt. Die Anwendung wurde mit MATLAB simuliert und im Anschluss mittels der Programmiersprache C implementiert. Um die RTT-Messwerte extrahieren, und sie weiters in einer Auswerteeinheit verarbeiten zu können, wurde der auf den RSUs eingesetzte ITS-G5 Protokollstapel modifiziert. Dabei wurde darauf geachtet, den Einfluss der Lokalisierungsanwendung auf die Hauptfunktionalität der RSU möglichst gering zu halten. Im Zuge von drei AuSSenbereichs Messkampagnen wurden verschiedene RSU Positionen, unterschiedliche Antennen und Übertragungsparameter getestet. Im Anschluss jeder Testreihe wurde mit den gewonnenen Erkenntnissen die Software weiter verbessert. Es zeigte sich, dass Mehrwegeausbreitung einen signifikanten Einfluss auf die Positionsschätzgenauigkeit hat. Nur unter nahezu idealen Bedingungen ist es möglich eine genaue Lokalisierung zu erhalten. Unter realen Bedingungen ist daher der Einsatz der Anwendung nicht praktikabel. Eine Kombination von RTT Messwerten und der Empfangssignalstärke, beziehungsweise die Verwendung einer zusätzlichen RSU könnte die Schätzgenauigkeit erheblich verbessern.

Acknowledgment

First, I would like to thank my mother and father for always supporting me and believing in me. Big thanks to my sister Gabi, my brother-in-law Michi and my two nephews Paul and Simon, for backing me up whenever I needed them.

I also want to thank the entire team of the Kapsch Solution Center Connected Roads for always freeing up some time to help me out (which happened more than once...) and giving me valuable support. Special thanks go to Heinz and Mats for all the nice discussions.

Many thanks to Prof. Mecklenbräuker for supervising my work. He provided qualitative feedback and enabled the cooperation between TU Wien and the Kapsch TrafficCom.

Last but definitely not least, I want to thank my fellow student, flat mate, and friend Harald. I could always rely on him, whether it was study-related or having a hop juice in the evening after a long day.

Contents

1 Introduction 2

1.1 Cooperative Intelligent Transport Systems: C-ITS . . . 3
1.2 Problem Statement . . . 4
1.3 Organization of the Thesis . . . 6

2 Localization Techniques 7

2.1 Localization Process . . . 8
2.1.1 Position Computation . . . 8
2.1.2 Location Parameter Estimation . . . 11
2.2 Vehicle-to-Infrastructure Localization Techniques . . . 14
2.2.1 Global Navigation Satellite Systems . . . 14
2.2.2 Vehicle-to-Infrastructure specific Localization Techniques . . . 15

3 802.11p 17

3.1 Orthogonal Frequency Division Multiplex (OFDM) . . . 18
3.1.1 Principles of OFDM . . . 18
3.1.2 Cyclic Prefix . . . 19
3.1.3 OFDM transmission chain . . . 20
3.1.4 Key IEEE 802.11p parameters . . . 21
3.2 Medium Access Control . . . 22

4 Vehicle Wireless Channel Propagation 25

4.1 Propagation Mechanisms . . . 25
4.1.1 Path Loss . . . 26
4.1.2 Doppler effect and frequency dispersion . . . 27
4.1.3 Scatters . . . 28
4.2 Statistical Description of Wireless Channels . . . 28

5 Position Estimation Application 34
5.1 Application description . . . 34
5.1.1 Application overview . . . 35
5.1.2 Preliminary Considerations . . . 35
5.2 Application Simulation . . . 43
5.2.1 Mathematical Computations . . . 44
5.2.2 Simulation . . . 48
5.3 Implementation . . . 50
5.3.1 Localization RSU Implementation . . . 51
5.3.2 Main Evaluation Unit Implementation . . . 53

6 Measurements 54
6.1 Pseudorange measurements . . . 55
6.2 2D position estimation . . . 56
6.2.1 Teesdorf measurements . . . 56
6.2.2 KCO measurements I . . . 59
6.2.3 KCO measurements II . . . 63

7 Conclusion 66

Bibliography 68

1

Introduction

The increasing need of transport systems or mobility in general during the last decades, naturally dragged along the problem of a raise in traffic. More accidents, transport delays and a higher pollution caused by vehicles, to name a few, are the result. Intelligent Transport Systems (ITS) try to tackle this problem by "utilizing synergistic technologies and systems engineering concepts to develop and improve transportation systems" [35]. ITS employs mobile, wireless and satellite technologies to provide a set of tools to increase transport efficiency, mobility, productivity and most importantly, road user safety. Intelligent Transport Systems can be segmented into three typologies [5]:

- Infrastructure Based Systems
  Aim to improve sustainability and network management. E.g. sensors, placed along the roadside to gather traffic- information in combination with user-warning and information equipment like Variable- message signs or managed motorways.
- Vehicle Based Systems
  Use telematics and in-vehicle technologies to provide safety based services to drivers. They are segmented into active (adaptive cruise control, lane keeping assistance, pedestrian detection systems) and passive (crash data recorders, external airbags, seatbelt load limiters) systems.
- Public Transport Based Systems
  Provide information and connectivity for passengers and operator. Examples are journey planning, smart ticketing and smart cards.

The European ITS Directive 2010/40/EU [12], applied since 26 August 2010, has accelerated the ITS deployment in the EU. It was released to step up the coordinated development of interoperating ITS services within the EU. Ex-post evaluations of the directive showed good results and with even better forecasts depending on the level of ITS services deployed. Among other things, Ursa Major, a test corridor combining the most economic regions from Rotterdam to Sicily, with 5000 participants taking part, reported a reduction of 51% of rush hour car trips. According to [28], the implementation of automated emergency call systems (eCall) has the potential to reduce road accidents with lethal consequences by 7000 lives and mitigate more than 70000 severe injuries over a 20-year span.

1.1 Cooperative Intelligent Transport Systems: C-ITS

Cooperative Intelligent Transport Systems (C-ITS) is the framework for communication between vehicles to vehicles and vehicles to infrastructure/pedestrians, combined in the collective term Vehicle-to-Anything (V2X). The term V2X combines:

- Vehicle-to-vehicle communications (V2V)
- Vehicle-to-infrastructure communications and vice versa (V2I/I2V)
- Vehicle-to-pedestrians communications (V2P)

The goal of C-ITS is the wireless data-interconnection between vehicles and transport infrastructure, pedestrians and other vehicles to enable a higher efficiency and road user safety compared to a single ITS service. The difference between ITS and C-ITS is that ITS are the tools providing intelligence whereby C-ITS focuses on the vehicle-to-anything connection.
An overview of C-ITS can be seen in Figure 1.1. Data from vehicles equipped with On Board Units (OBU) either directly to other users or via a Road Side Unit (RSU) to the Traffic Management Center, which processes it and takes intelligent actions to increase transport efficiency and user safety.
Due to the ability to gather information about traffic disruption from C-ITS stations in almost real-time, target orientated warnings for approaching road users, increase traffic safety.
ITS and C-ITS are an essential component of connected and autonomous vehicles, smart cities, integrated transport systems and Mobility as a Service (MaaS).

C-ITS Communication Standards

Within C-ITS there are specific standards introduced for the communication between vehicles-to-anything. There are two different technologies with inherent standards: Cellular - V2X (C-V2X) and Dedicated short-range communications (DSRC). C-V2X is based on cellular mobile networks and is standardized by the 3rd Generation Partnership Project (3GPP). DSRC, on

the other hand, is a technology-based on the wireless LAN standard Institute of Electrical and Electronics Engineers (IEEE) 802.11. The main participants for pushing the V2X development using DSRC are the EU,US, and Japan. Since the individual countries follow different objectives for the V2X deployment, each region deploys its standards.

Europe

The European Telecommunications Standards Institute (ETSI) adapted the IEEE 802.11p standard (further referred to as 11p) according to the European requirements and released it under the name ITS-G5 (see [11]). In Europe, the Car-to-Car Communications Consortium (C2C-CC), a consolidation of vehicle manufactures, equipment suppliers and research institutions [4] works on the research and development of C-ITS solutions and is together with ETSI, the main member for moving forward cooperative intelligent systems. In 2008 the EU allocated 30MHz in the frequency band from 5.875 - 5.905GHz for safety-related ITS applications ([11])

US

In the US, the IEEE is responsible for standardization regarding communications. As in the EU, the American protocol stack is based on 11p. The collective term for the US specific protocol stack is referred to Wireless Access for Vehicular environment (WAVE). A 75MHz wireless spectrum in the 5.9GHz frequency range is allocated for ITS services using DSRC by the Federal Communications Commission (FCC) [8].The main driving force for ITS deployment is the United States Department of Transportation (USDOT), working with the industry and public stakeholders jointly together to further ITS solutions.

Japan

Japan has two dedicated ITS frequency bands, defined by the Association of Radio Industries and Business (ARIB). One exclusive and licensed, in the 755.5- 764.6MHz band and the one in the range from 5.770 to 5.850GHz band, used for Electronic Toll Collection (ETC). Compared to countries in the EU and US, ITS is widely installed in Japanese vehicles (more than 60 million cars [1]), mainly for ETC.

1.2 Problem Statement

A significant part of ITS is the determination of the precise location of users in the transport network. Especially for safety-relevant applications like vehicle collision warning systems, vision enhancement, or autonomous-driving vehicles, high accurate position information is needed. Commonly a global navigation satellite system (GNSS) is used to provide the vehicle position. Therefore a GNSS receiver and at least three or more GNSS satellites, which are in line of sight to the receiver, are needed. The standard GNSS position determination can be improved by

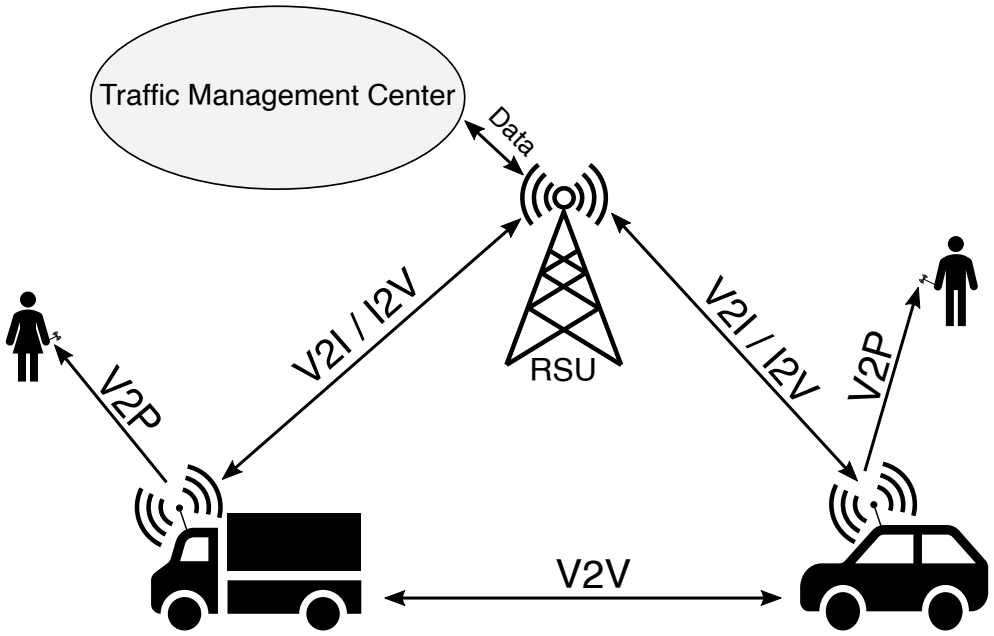

Figure 1.1: C-ITS Overview

correction procedures like the Real-Time Kinematic method, which increases the accuracy down to a range of centimeters.

In practice, the satellite signals interfere with other radio frequencies, get distorted by obstacles like buildings, dense foliage, or mountains. Especially when driving through tunnels or in parking garages, a GNSS system is likely to suffer from persistent outages.

The Angle of Arrival (AoA) position estimation method circumvents the need for an external satellite signal. For the estimation of the arrival angle, an antenna array at the receiver is needed. The estimation is done by measuring the phase differences when the incident signal impinges the different antenna elements. To get a two- dimensional position fix, given that the receiver is placed in a known height above the object which has to be localized, it is sufficient to estimate the angle of arrival towards the x and y-axis.

Although this method delivers accurate position estimates in good conditions (line of sight, short distance between receiver and target), the estimates worsen when using this method in the field. Shadowing effects and multipath propagation due to obstacles in the signal path influence the estimation.

A different approach is based on the propagation time between transmitter and receiver. Assuming that the propagation speed is constant and independent of the position, the range is calculated as the product of time of flight and propagation speed. In the simplest case, the location is determined via triangulation. One approach is that the targets transmit a wireless frame, and the receiver passively listens. To calculate the time of flight, the exact time when the frame was transmitted has to be known. This method requires precise synchronization between the transmitter and receiver to allow an exact estimation of the location. Instead of measuring one

way, the round trip time (two-way method) can be utilized, which eliminates the need for precise synchronization. A promising approach based on the paper [6] is, to use the acknowledgment (ACK) frame in the 11p protocol, which acknowledges the successful reception of a transmitted frame. Since the egress time of the frame is determined by the transmitter, the round trip time can be measured by using a timer/counter.
This approach gets along without synchronization of transmitter and receiver. Since the ACK frame is inherent to the IEEE 802.11 protocol, it is easily implemented in existing systems and is not limited to 11p. The goal of this thesis is to implement a time-based localization method in an already existing system and evaluate its performance in regards to accuracy and resilience to multipath propagation and shadowing.

1.3 Organization of the Thesis

The structure of this thesis is a following: The first chapter should give the reader a broad overview on Intelligent Transport Systems and their deployment in the real-world, followed by a short problem statement, describing what the initial problem, this thesis is supposed to solve. The second chapter lists and describes standard position localization techniques, where they are used and their properties, including the chosen techniques for this thesis. Chapter three gives an overview of the IEEE 802.11p standard, in which the application described in the fifth chapter, is implemented. The fourth chapter describes which effects signals experience when traveling over a wireless channel and models, which can be used to describe these effects. Afterward, the implemented application and the associated Matlab simulations are presented, followed by real-world measurements, taken with Kapsch's Road Side Units and states the problems, possible improvements, and the results. The final chapter, seven states the conclusions that can be drawn.

2

Localization Techniques

Radio localization has been around for many years and has gained in significance ever since. Especially with the emerge of Wireless Sensor Networks (WSN), where the sensor position is often not known *a priori*, the location's determination is crucial to provide a physical context to sensor readings. State-of-the-art localization techniques are still based on the same principles used in the early stages and have not lost their importance. The following two sections are structured as follows: Section 1 gives an overview of localization processes and the steps required to get a position estimation, including a summary of geometries in localization methods. Section 2 presents the probably most widely used position estimation technique, Global Navigation Satellite Systems, and two novels, GNSS-free Vehicle-to-Infrastructure specific Localization Techniques.

2.1 Localization Process

The process of estimating the location always comprises an exchange of signals between the target and one or several base stations (STA) with known positions. There are two distinct ways of how this can be done. If the position is directly, thus, in one step, extracted from the received signal, the method is termed Direct Position Determination (DPD). If there is a preceding intermediate stage between the received signal and the location estimate, the process is referred to as a Two-Step Position Determination. In the former case, it mostly reduces to solving a Least-Square (LS) minimization problem respectively if the noise is assumed to be Gaussian, a maximum likelihood estimation. According to [36], DPD performs under high SNR scenarios as good as a Two-Step Position Determination but has a far superior accuracy at low SNR. However, the DPD is computationally expensive, which is why most techniques use a two-step approach, as shown in Figure 2.1. The two-step approach can be further segmented into three components [3]: Location parameter estimation, position computation, and tracking.

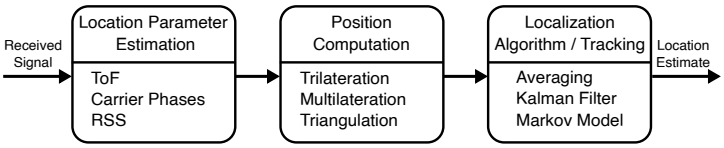

Figure 2.1: Localization Process: Two-Step Position Determination

After picking up the receive signal, the first step is to extract the bearing angles and ranges. For this purpose, different methods such as Time of Flight (ToF), Received Signal Strength (RSS), or the evaluation of phase differences in the detected carrier using an Angle of Arrival Method can be utilized. The so gathered location parameters are further used to compute the target's position via trilateration, multilateration, or triangulation techniques. The main part of the localization process is done in the final stage, where the previously calculated estimations are filtered using simple averaging filters, Kalman filtering, or more elaborate approaches as Neural Networks [20].

2.1.1 Position Computation

The first step of a localization process is estimating the location parameters, namely the bearing angles and the ranges between target and STAs. If only the range- information is used or available for localizing, trilateration or multilateration techniques come into use. If the chosen option is based on bearing angles, triangulation provides a solution. However, every combination of bearing angles and range estimations can be used to get a first localization estimate.

Trilateration

The most straightforward geometric approach to find the target location when only the distances between target and STAs is known is triangulation. For this purpose, the intersection points of multiple, non-collinear circles are calculated. The radii are given by the ranges obtained from the received signals. For an unambiguous position fix in the two-dimensional plane, the distance to at least three STAs has to be known. In the setup shown in Figure 2.2, the three stations STA_1, STA_2 and STA_3 are placed at $(x_1/y_1)^T$, $(x_2/y_2)^T$ and $(x_3/y_3)^T$. The to be localized target T is at the intersection point at $(x_T/y_T)^T$. T is d_1 away from STA_1, d_2 from STA_2 and d_3 from STA_3. The distances d_i with $i = 1 \dots 3$ are calculated as:

$$d_i = \sqrt{(x_i - x_T)^2 + (y_i - y_T)^2} \tag{2.1}$$

It is possible to estimate the position using only two STAs; however, there will be two ambiguous solutions. Since the distance measurements are erroneous in practice, the circles do not intersect at one point; instead, there is an overlapping area. This location uncertainty can be dealt with using LS optimization [37]. Furthermore, it should be noted that the three circles do not necessarily intersect at all.

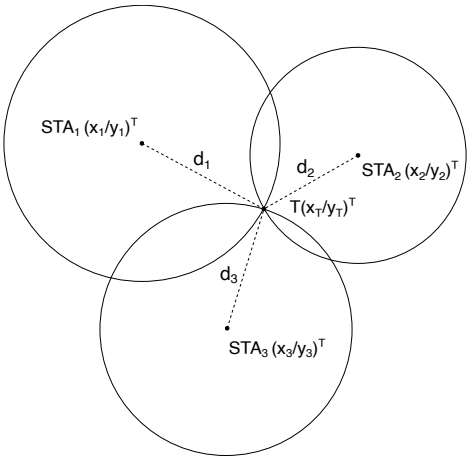

Figure 2.2: Trilateration: Position estimation in the two-dimensional plane using three STAs

Multilateration

Depending on the method used in trilateration, target and STAs have to cooperate in order to get a position estimation. When using an RSS approach, the transmit power has to be known to deduce from the received signal strength to the range between target and STAs. In a ToF approach, the exact transmit time and highly synchronized STAs, among themselves and target are prerequisites. In the case of round trip measurements, the turnaround time between receiving the signal and responding must be known. Multilateration uses a similar principle as trilateration, although instead of ranges, the time distinction in the arrival of signals is

used for localization. STAs have to be synchronized among themselves, but the cooperation between STAs and target is not required. In the case of multiple targets, each target has to be uniquely identifiable. Assuming that the position estimation is done on the station-side, the target transmits a beacon received by the STAs. For each STA pair, the range differences, retrieved from the time differences, result in an infinite number of possible positions that form a hyperbolic curve. The intersection between the hyperbolas localizes the target position. In Figure 2.3 an example using three STAs, STA_1, STA_2, and STA_3, intersecting in one point T at $(x_T/y_T)^T$ is shown. Because no cooperation between STAs and target is needed, multilateration is one of the most commonly used techniques, deployed among others in surveillance- and radio-navigation systems [22].

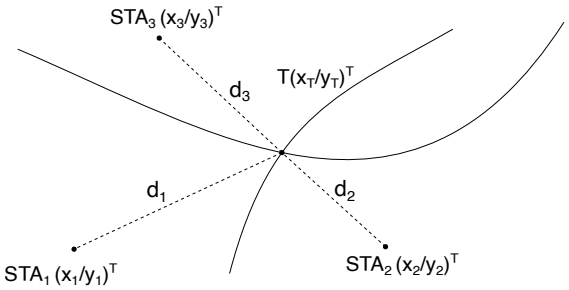

Figure 2.3: Multilateration: Position estimation in the two-dimensional plane using three STAs

Triangulation

Compared to the previously stated trilateration and multilateration, triangulation uses angular measurements to determine the target location. For this, the direction to the target is estimated using Angle of Arrival (AoA) techniques. The intersection points are obtained using the angles in a triangle, as shown in in Figure 2.4. Here, α_1 and α_2 denote the angles from STA_1 respectively, STA_2 to the target T with respect to the x-axis. As long as the estimated target is not on the direct line connecting the stations, the solution is always unambiguous.

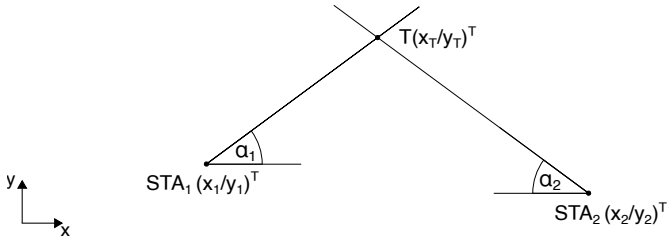

Figure 2.4: Triangulation: Position estimation using angular measurements

2.1.2 Location Parameter Estimation

An essential step in the position estimation process is extracting the localization parameters from the received signal. They form the foundation of the subsequent processing steps. The most common measurement techniques can be classified into three groups: Received Signal Strength (RSS) based methods, time-based measurements, and Angle of Arrival techniques [13].

Received Signal Strength

Estimating the distance between STA and target using the Received Signal Strength (RSS) is a widely used technique because it does not require additional hardware and can be easily implemented. It is based on Friis transmission formula for free-space propagation Section 4.1.1 which states the relationship of the receive power $P_{RX}(d)$ to the transmit power P_{TX} as:

$$P_{RX}(d) = P_{TX} G_{TX} G_{RX} \left(\frac{\lambda}{4\pi d} \right)^2 \tag{2.2}$$

where G_{TX}, G_{RX} is the transmitter antenna gain respectively the receiver antenna gain, λ the transmit signal wavelength and d the distance between transmitter and receiver. However, this idealized model does not take propagation effects such as scattering, diffraction, or reflection into account. A simple model, including these mechanisms, is the log-distance path model:

$$P_{RX}(d)|_{dBm} = P_{RX}(d_0)|_{dBm} - 10\gamma \log_{10} \left(\frac{d}{d_0} \right) + X_\sigma|_{dB} \tag{2.3}$$

where $P_{RX}|_{dBm}$, $P_{RX}(d_0)$ denotes the receive power at a distance d respectively at a reference distance d_0 in dBm, γ, the path loss exponent which is normally in the range between $2-4$, where 2 is for free-space propagation and 4 for relatively high-loss environments and X_σ denotes a random variable with a standard deviation σ in decibels. For slow-fading, X_σ may be Gaussian, for fast-fading Rayleigh- or Rician distributed. In the case of no fading at all, X_σ is set to zero. In general, there is a distinction between empirical models and deterministic models, which are based on the physical law of wave propagation. There are also combinations of both types, known as semi-empirical models. Examples for the most common empirical models are the Okumura and COST-231 Hata model, for deterministic models among others, the Ikegami model [31]. Deterministic models are very accurate but often not suitable for practical applications since they are computationally expensive and require a detailed and accurate description of the propagation environment which is often not available. On the other hand, empirical methods are obtained using extensive measurement campaigns and supply predictions only for predefined setups.

A different approach using RSS is the fingerprinting or profiling method. For this purpose, the RSS behavior is measured in the coverage area and stored in the form of a map. This is done *a priori* in an off-line training phase [23]. In order to reduce the amount of measurement points, additional information such as geometries and propagation laws can be used to refine the map.

In the on-line phase, the obtained RSS measurements are compared with the information stored in the map, and using position estimations algorithms, the location is determined. The profiling approach has the major drawback, that the map is only valid as long as the surroundings remain unchanged.

Time-based Measurements

In time-based measurements, the range between transmitter and receiver is found by assuming that the wave propagates in an isotropic medium with a constant propagation speed c. Multiplying the Time of Flight (ToF) with c delivers a range estimation, the *pseudorange*. Time-based measurements can be further grouped into Time of Arrival (ToA) and Time Difference of Arrival (TDoA) techniques.

Time of Arrival

The Time of Arrival (ToA) method is the most straight forward approach in time-based measurements. The difference between transmitting and receiving the frame is multiplied by the propagation speed to obtain a range estimation. ToA ranging can be done either one-way (OW-ToA), where the STA transmits a wireless frame, and the target captures the time it received it or Two-way (TW-ToA), where the round trip time (RTT) is taken. This eliminates the need for exact synchronization. In the former case, the STA and target have to be accurately synchronized, and the information when the transmitter sent the frame has to be known. Even slight offsets in the range of nanoseconds cause estimation errors of several meters, making the OW-ToA approach less attractive. In the TW-ToA, the target receives a frame and returns the signal after a specified amount of time. Since only one clock is used for measuring the round trip time, synchronization is not a problem. Although the turnaround time at the target-side has to be precisely known. Several approaches have been proposed for gathering this information via either a calibration process or the target sends its turnaround time to the STA, where it is then subtracted from the RTT [25].

Time Difference of Arrival

Given that cooperation between STA and target is not possible, the location can be estimated using a Time Difference of Arrival (TDoA) technique using multilateration (see Section 2.1.1). It does not require knowledge of the turnaround time, nor a synchronization between target and STA. Assuming a scenario where four stations, STA_i, $i = 1 \dots 4$ estimating the position and a target T transmits a signal (i.e., a beacon) which is received by all stations, the time difference Δt between a pair of receivers, STA_i and STA_j is then given by [23]:

$$\Delta t_{ij} \widehat{=} t_i - t_j = \frac{1}{c}(\|STA_i - T\| - \|STA_j - T\|),\ i \neq j \tag{2.4}$$

where c denotes the propagation speed, $\|\cdot\|$ the Euclidean norm and t_i, t_j the time when the signal is received. A widely used approach to measure the TDoA is to calculate the argument t, which maximizes the cross-correlation R_{ij} function:

$$TDoA = \max_t |R_{ij}(t)| = \max_t \left| \int_{-\infty}^{\infty} {s_i}^*(\tau) s_j(t+\tau) d\tau \right| \tag{2.5}$$

Here, ${s_i}^*$ denotes a complex-conjugate signal, received by STA_i and s_j the signal received by STA_j. Using a TDoA approach requires an accurate synchronization between the STAs but does not impose any signal restrictions. An increase of the STA spacing will improve localization accuracy since this leads to a wider time-of-arrival spacing. TDoA positioning can also be applied for audio signal source localization.

Angle of Arrival

The third category of location parameter methods are based on the Angle of Arrival (AoA). In combination with triangulation methods (see Section 2.1.1), the position can be estimated using the bearing angles. AoA methods are split into two categories: Beamforming and phase interferometry. Beamforming uses a highly directional antenna, where the anisotropy of the reception pattern (Figure 2.5) is used to extract the angular information. The antenna is rotated either mechanically or electronically, and the direction where the maximum receive power is detected corresponds to the transmitter's direction. This technique is prone to be sensitive to receive power fluctuations since the antenna cannot see whether the signal varies due to fluctuations or if it is due to the anisotropic radiation pattern. Phase interferometry, on the other hand, uses spatially spaced antennas, which detect phase differences in the phase front arrival. An example using three receive antennas, uniformly spaced with a distance d, is shown in Figure 2.5. Assuming that the incoming phase front is considered to be planar, the AoA α is calculated as:

$$\alpha = \arcsin\left(\frac{a}{d}\right) \tag{2.6}$$

where a is the path difference and l the antenna spacing. Different approaches have been proposed to estimate the phase difference, among others, using the time- or phase- differences of the received signal. Limited directivity of antennas, shadowing, and multipath propagation are constraining factors when using AoA measurements.

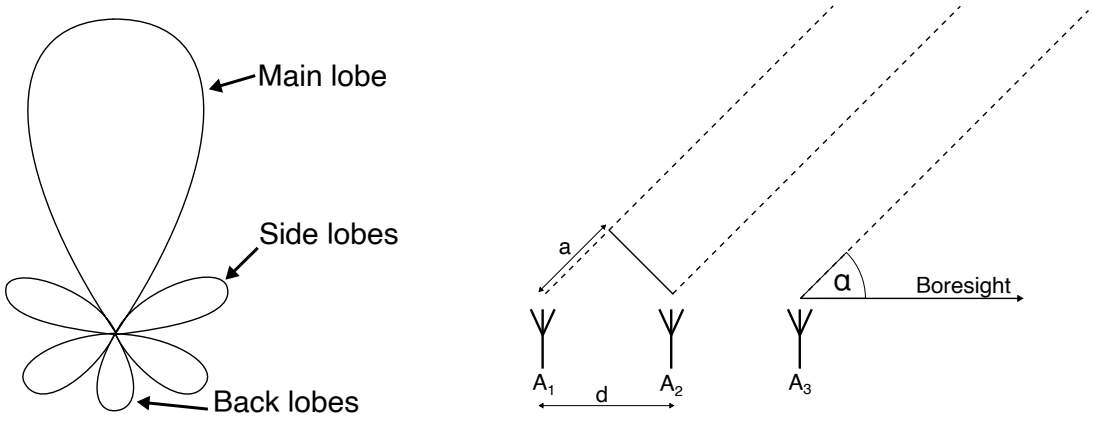

Figure 2.5: Left: Typical directional antenna radiation pattern, right: antenna array with multiple antennas forming an phase interferometer

2.2 Vehicle-to-Infrastructure Localization Techniques

A variety of localization technologies have been researched, developed, and are already employed in the field. This section gives an overview of a few state-of-the-art techniques used in Vehicle-to-Infrastructure (V2I), starting with Global navigation satellite systems (GNSS) and followed by a comparison of two newly introduced localization techniques specifically for V2I applications.

2.2.1 Global Navigation Satellite Systems

Global navigation satellite systems (GNSS) uses satellites to provide a geo-spatial position estimation. The fields of application are manifold, from military use for weapon systems to civil applications for vehicular navigation. One of the most known GNSS is the American Navigational Satellite Timing and Ranging - Global Positioning System (NAVSTAR-GPS), nowadays referred to as GPS. Other nations also run satellite-based navigation systems, such as China, which deploy BeiDou, the European Union, Galileo, and the Russian Federation, GLONASS. GNS systems have an estimation accuracy from a few meters to above 20 m [33]. Each satellite transmits coded radio signals in the spectrum between 1.2 and 1.6 GHz, the so-called L2- respectively L1 -band that contains their actual position and the exact time. The GNSS carriers are modulated with a pseudorandom noise (PRN) code, which is a binary code without any obvious pattern. Repeating this code interval every few milliseconds enables to measure the signal transmission time. Therefore, the receiver generates a local replica of the PRN code and compares it continuously with the received signal, as shown in Figure 2.6. Multiplying the so found time τ with the propagation speed yields to a pseudorange. Using multilateration methods further on, the position can be estimated. The PRN code also serves as a unique fingerprint to identify the individual satellites. In theory, three satellites would be sucient to calculate the spatial position; however, unsynchronized clocks lead to synchronization issues, which are solved by tracking a

fourth satellite. GNS systems can also determine the velocity via measuring the change in the received frequency caused by the Doppler effect [34].

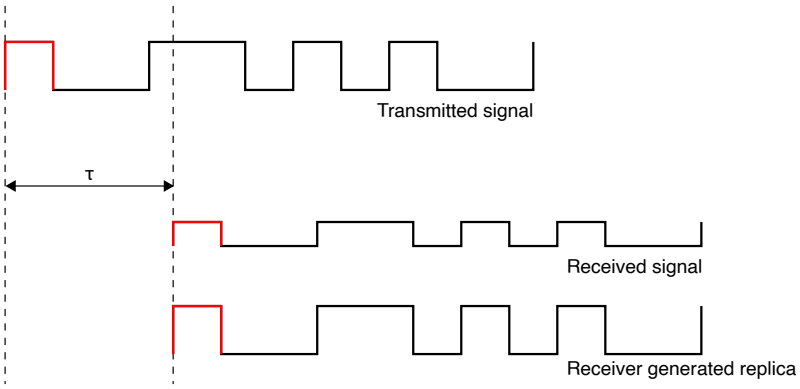

Figure 2.6: Range estimation using pseudorandom noise codes

External factors can largely influence the achieved accuracy of GNS systems. Multipath propagation, urban canyon environments, or when the radio signals pass through the tropo- and ionosphere, to name a few. One way to minimize the error and achieve higher accuracy is to use a Differential GPS (DGPS) setup. The goal here is to reduce the error introduced by distorted propagation delays via providing information used to correct the biases mathematically. The correction data is typically sent from a reference-station that knows its exact position and calculates the difference between the actual and estimated position. This correction data is then sent to DGPS receivers nearby. Using DGPS, a positional accuracy of 1 cm – 5 cm is achievable [34].

2.2.2 Vehicle-to-Infrastructure specific Localization Techniques

This section presents two novels GPS-free, V2I specific localization techniques, stating their advantages and disadvantages. The authors of [14] proposed a GNSS- free localization technique, exploiting V2I communications. Therefore, the AoA of beacon packets sent by a roadside unit (RSU) combined with the RSU's position information, which is included in the beacon, is used to estimate the position. Using Monte Carlo simulation, the approach was tested following the ETSI standard [10] at a carrier frequency $f_c = 5.9\,\text{GHz}$, a bandwidth of $B = 10\,\text{MHz}$ with a transmit power $P_T = 18\,\text{dBm}$. It delivered good results for high SNR values even within multipath environments. With increasing RSU to target distance, the performance decreased and obtained at an approximate distance of 155 m a GPS- level accuracy. The proposed approach does not need any sensors or a GPS signal but requires short RSU to target distances for accurate estimations. In the paper from Del Peral-Rosado *et al.* [27], 5G networks' feasibility for localization was studied. The focus was laid on multicarrier and TDoA measurements. A highway scenario was simulated, with base stations deployed every 200 m. Using a bandwidth

$B = 20\,\text{MHz}$, an accuracy below 5 m was achieved, increasing the bandwidth to 50 MHz, and up to 100 MHz resulted in an accuracy of below 25 cm, respectively 20 cm in 99 % of the cases. Non-line of sight conditions limits the ultimate position accuracy. The main cost of the system is the implementation of 5G base stations.

3

802.11p

IEEE 802.11 presents a set of standards, published by the Institute of Electrical and Electronics Engineers (IEEE), which specifies the medium access control (MAC) and the physical (PHY) layer for the implementation of wireless local area networks (WLAN). IEEE 802.11p is an amendment of IEEE 802.11a, specifically designed for the needs of connected vehicles such as C-ITS. 802.11p enables data exchange between fast-moving vehicles to other vehicles and roadside units in the licensed ITS band at 5.850 GHz – 5.925 GHz with a channel spacing of 5 MHz, 10 MHz and 20 MHz. It operates on nine channels, starting with channel 172 at 5.86 GHz up tp channel 184 at 5.92 GHz. Channel 174, 176 and 180, 182 can be combined to form 20 MHz channels namely channel 175 respectively 181 [2]. Since almost exclusively 10 MHz channels are used for C-ITS applications, the following chapter is mainly focused on these.

IEEE 802.11p includes mandatory support of 6, 12 and 24 Mbps transmit data rates. It optionally supports 9, 18, 36, 48 and 54 Mbps data rates. For modulating the carriers, binary phase-shift keying (BPSK), quadrature phase-shift keying (QPSK), and 16-quadrature amplitude modulation (QAM) and 64-QAM are used. To improve the error rate, forward error-correcting codes (FEC) are employed. Therefore, the sender adds redundant bits to the code which allows the receiver to correct errors. A measure of how much redundant code n in proportion to the data which carriers useful information k is given by the coding rate $R = k/n$. In Table 5.1 the supported rates and modulation schemes for 10 MHz channels are shown.

Modulation Type	BPSK		QPSK		16-QAM		64-QAM	
Coding rate	1/2	3/4	1/2	3/4	1/2	3/4	2/3	3/4
Coded bit rate	6 Mbps		12 Mbps		24 Mbps		36 Mbps	
Data rate	3 Mbps	4.5 Mbps	6 Mbps	9 Mbps	12 Mbps	18 Mbps	24 Mbps	27 Mbps

Table 3.1: IEEE 802.11p: Supported Modulation schemes and data rates

3.1 Orthogonal Frequency Division Multiplex (OFDM)

The key PHY layer technology is Orthogonal Frequency Division Multiplex (OFDM). OFDM is a multicarrier transmission technique that separates the transmit data and distributes it onto several orthogonal narrowband subcarriers. Each subcarrier is in the nulls of all other subcarrier and therefore, does not interfere with others (see Figure 3.1). Compared to a single-carrier modulation scheme, OFDM is capable to deal with severe channel interference such as narrowband fading due frequency selective fading in multipath environments without the need for complex equalizers.

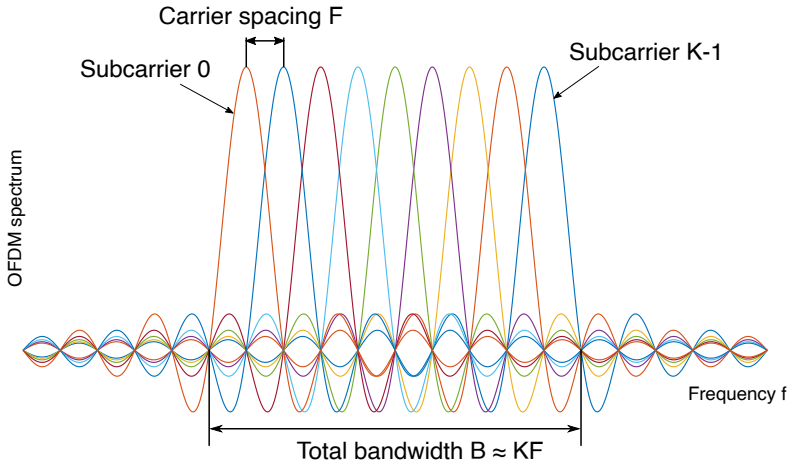

Figure 3.1: OFDM spectrum

3.1.1 Principles of OFDM

Instead of transmitting the data over a single carrier with bandwidth W, the data stream is split up into K parallel sub-streams. The input data is loaded up onto K different, sinusoidal carriers which are orthogonal to each other. In the simplest case, each carrier is placed F apart. Assuming rectangular transmit and receive pulses, given by

$$g_k(t) = \begin{cases} \sqrt{F}, & 0 \leq t < \frac{1}{F} \\ 0, & \frac{1}{F} \leq t < T \end{cases} \tag{3.1}$$

where T is the symbol duration [24], a single OFDM symbol can then be written as:

$$s_n(t) = \begin{cases} \sqrt{F}\sum_{k=0}^{K-1} x_{n,k} e^{j2\pi kFt}, & 0 \leq t < \frac{1}{F} \\ 0, & elsewhere \end{cases} \tag{3.2}$$

Here $a_k[n]$ denotes complex- valued symbols, in the $n-$th time-interval, on the $k-$th subcarrier. The transmit signal $s(t)$ is calculated as the summation of the time- shifted OFDM symbols $s(t) = \sum_n s_n(t - nT)$. To ensure orthogonality of the carriers, the pulse duration $1/F$ has to be smaller than T (see Figure 3.2) or equivalently, the product $TF \geq 1$. If this is not the case, it may result in Inter Symbol Interference (ISI) subsequently that the receiver is not able to reconstruct the transmitted information. However, a larger time-bandwidth product TF would reduce ISI but it is unfavorable since it worsens the spectral efficiency. In practical systems, a trade- off value for TF between spectral efficiency and ISI reduction of 1.02...1.25 is used [24].

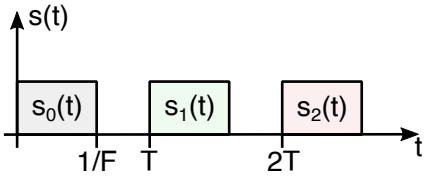

Figure 3.2: Transmit signal

It has shown that it is beneficial, to switch from a time- continuous to a time- discrete description for the implementation of an OFDM system. Sampling the transmit signal $s(t)$ at a period $T_S = 1/B$, yields to a discrete- time signal $s[m] = s(mT_s)$, where m denotes the discrete time, which can be written as the summation of the single discrete-time OFDM symbols as following:

$$s[m] = \sum_n s_n(m - nN) \tag{3.3}$$

where N is the discrete-time symbol duration and $s_n[m]$ the OFDM symbol:

$$s_n[m] = \frac{1}{\sqrt{K}} \sum_{k=0}^{K-1} x_{n,k} e^{j2\pi \frac{km}{K}} \tag{3.4}$$

We see, that (3.4) is the inverse Discrete Fourier Transformation (DFT) of $x_{n,k}$ with a sample size K. In practice, a sample size to the power of two is chosen which enables an effective implementation using inverse fast Fourier transformations (IFFT) respectively FFT algorithms on the receive side.

3.1.2 Cyclic Prefix

Assuming the OFDM signal passes trough a multipath channel with a discrete-time Finite-Impulse Response (FIR) $h[l]$ of length L, disregarding noise effects, the received signal can be expressed as the following linear convolution:

$$r[m] = (h * s)[m] = \sum_{l=0}^{L-1} h[l]s[m-l] \tag{3.5}$$

As long as $L-1 \leq N-K$, ISI is avoided (see Figure 3.3) but if delayed copies of the preceding symbol interfere with the current symbol, information could get lost, since the receiver may not be able to retrieve the original data.

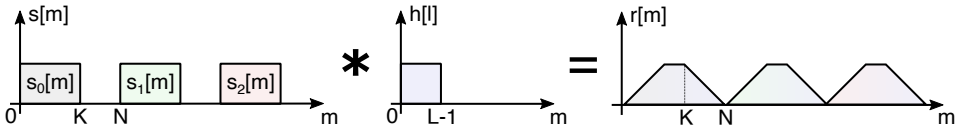

Figure 3.3: Input signal $s[m]$ linear convoluted with the channel $h[l]$

This can be circumvented by individually prefixing a copy of the end part of the OFDM symbol to the beginning (see Figure 3.4) of it. That acts as a guard band between the symbols and enables to turn the linear convolution, to be modeled as a circular convolution. The received cyclic prefixed OFDM symbols can be stated as $\tilde{r}_n[m] = (s_n \circledast h)[m]$ with:

$$\tilde{r}_n[m] = \begin{cases} r[m+nN], & 0 \leq m < K \\ 0, & elsewhere \end{cases} \tag{3.6}$$

The receiver discards the signal during the interval between consecutive symbols (3.6) to eliminate ISI. Due to the cyclic prefixed OFDM symbols, they appear periodic after convolving it with the channel impulse response. This corresponds to a multiplicative input-output relation between transmit signals $x_{n,k}$ and receive signals $y_{n,k}$ in the time domain:

$$y_{n,k} = DFT_{m \to k}\{\tilde{r}_n[m]\} = H_k x_{n,k} + z_{n,k} \tag{3.7}$$

where H_k is the DFT of the channel impulse response $h[l]$ and $z_{n,k}$ additive white and Gaussian noise terms. Henceforth, a single carrier is only effected by a single channel coefficient. As long as the channel is time invariant over the duration of one OFDM symbol, (3.7) holds.

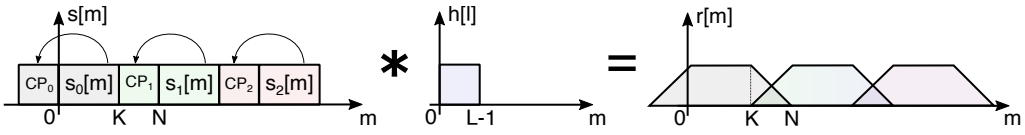

Figure 3.4: OFDM symbols with attached cyclic prefix (left), sent over a channel with impulse response $h[l]$ (middle). Receive signal $r[m]$ (right) with overlapping cyclic prefixes

3.1.3 OFDM transmission chain

Having discussed the basic principles of OFDM, we can take a look at a simple OFDM transmission chain as shown in Figure 3.5. At the **transmitter**, the input data stream is first mapped to

a symbol stream using a constellation modulator (compare with Table 5.1). In the next stage, the data is split up into K parallel streams using a *Serial-to-Parallel Converter*. At this point, the frequency domain symbols $X[0] \dots X[K-1]$ are transformed into the time domain using an IFFT. Before being serialized again, a cyclic prefix is added to circumvent ISI. The CP overhead is based on the delay spread introduced by the channel. Adding a CP decreases the data rate by $CP/(K+CP)$. The length of CP is always a trade-off between the robustness of the transmission and rate loss. The OFDM symbol is obtained after the *Parallel-to-Serial Converter*. It is $(K+CP)T_S$ long and able to withstand a delay spread of at most $(CP+1)T_S$. In the radio frequency (RF) stage, the digital-to-analog converted symbols are used to modulate cosine and sine waves oscillating at the carrier frequency. On the **receiver** side, the signal is picked up by a receive antenna, downmixed and subsequently analog-to-digital converted. The so obtained data stream $y[n]$ is then split up in K parallel sub-streams. Here, the previously inserted cyclic prefixed is removed and the time domain symbols $y[0] \dots y[K-1]$ are transformed back into the frequency domain using a FFT. The symbols $Y[0] \dots Y[K-1]$ get serialized and demapped to obtain the original data back.

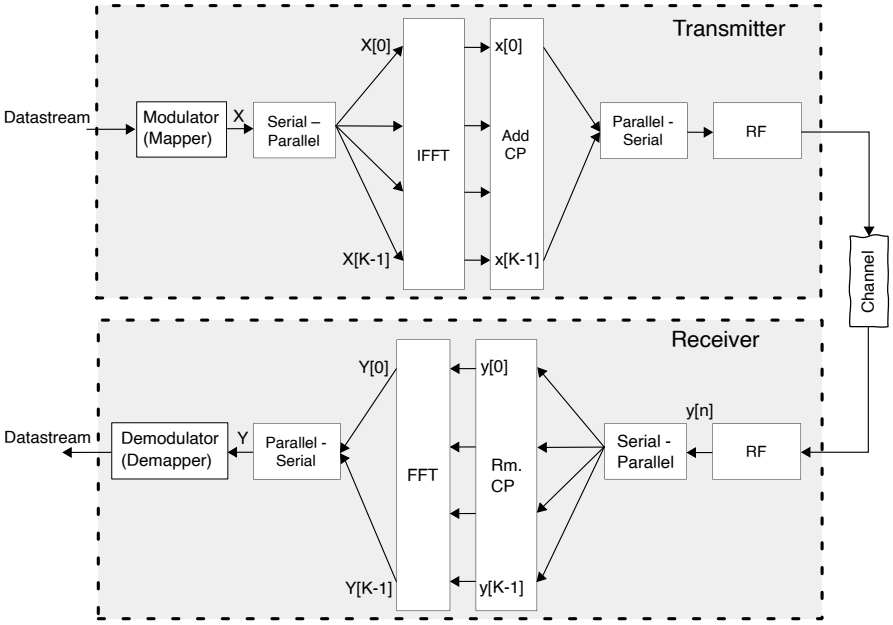

Figure 3.5: Simple OFDM transmission chain with cyclic prefix

3.1.4 Key IEEE 802.11p parameters

To meet the requirements demanded by V2X applications, such as handling communications at high relative speeds (up to 260 km h^{-1} [21]) and providing a reliable transmission in extreme multipath environments, the 802.11p amendment adapted parameters of the IEEE 802.11a Wi-Fi standard. The following table gives an overview of the 802.11p key parameters based on 802.11a [19]:

Parameter	IEEE 802.11a 20 MHz channel spacing	IEEE 802.11p 5 MHz channel spacing	IEEE 802.11p 10 MHz channel spacing	IEEE 802.11p 20 MHz channel spacing
Number of subcarriers	52	52	52	52
Subcarrier frequency spacing	312.5 kHz	78.125 kHz	156.25 kHz	312.5 kHz
Symbol duration	4 µs	16 µs	8 µs	4 µs
Guard time	0.8 µs	3.2 µs	1.6 µs	0.8 µs
FFT period	3.2 µs	12.8 µs	6.4 µs	3.2 µs

Table 3.2: IEEE 802.11: Overview key parameters

As it can be seen in Table 3.2, 802.11p uses a half-clocked mode for 10 MHz channels and quarter-clocked mode for 5 MHz channels. This increases the timing parameters time by a factor of two respectively four.

3.2 Medium Access Control

The MAC layer controls the access to the physical transmission medium which is in IEEE 802.11, the wireless channel. It is a multiple access method that allows for several stations (STA) to share the same medium. In combination with the logical link control (LLC) sublayer, which enables communication with the upper network layer and the lower MAC layer, they form the data link layer (DLL). For wired networks, like Ethernet, the common MAC layer standard is carrier-sense multiple access with collision detection (CSMA/CD) whereas, for wireless networks, it is CSMA with collision avoidance (CSMA/CA).

Carrier-Sense Multiple Access with Collision Avoidance

To avoid collisions, the carrier-sense multiple access algorithm with collision avoidance is implemented at each STA. Every STA shall sense the medium and wait until it is idle for a specified amount of time. In the case of the channel being busy, all other STA have to wait until the end of the current transmission. Before attempting to transmit again, each STA backs off for a random interval. Stations or services may be prioritized via a shorter backoff time using four different access categories (ACs). Starting with the lowest *Background, Best Effort, Video* and the highest being *Voice*. Individually addressed traffic (i.e. everything apart from broadcast messages) will be immediately acknowledged by an acknowledgment frame (ack frame) [19]. If no ack frame is received, the transmitter schedules a retransmission.

Acknowledgment procedure

Figure 3.6 shows a typical acknowledgment procedure. A STA (source) transmits after sensing an idle medium. The receiving STA (destination) waits for an specified amount of time, the interframe space (SIFS), before confirming the reception of the package with an ack frame. The

channel has to be idle for at least the time specified by the distributed coordination function interframe space (DIFS) before other stations may attempt to transmit. 802.11 uses ten different interframe spaces (IFS) to prioritize the medium access. The highest priority, therefore the shortest backoff time is reserved for the ack frame. For a 10 MHz channel, the SIFS is defined to be 32 µs ± 10%.

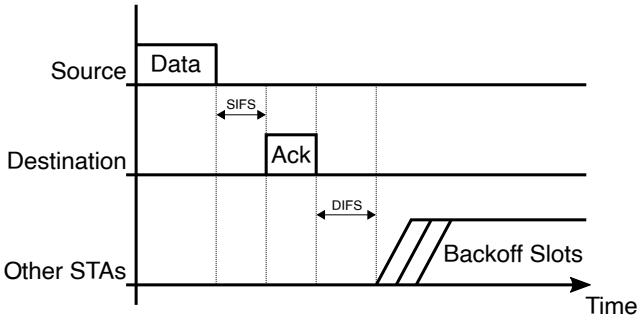

Figure 3.6: Acknowledgment procedure in IEEE 802.11

Acknowledgment Frame Structure

802.11 MAC frames consist of common fields, which are present in every frame and specific fields, which are dependent on the frame type. Every frame starts with the 10 bytes long MAC header which includes a frame control field, indicating which type of data is transported, the duration and the receiver address [16]:

Frame Control

The protocol version is set to 00 (the current protocol version is 0), the type field is set to 01 which indicates that the frame is a control frame instead of a data frame. To further show that the frame is an ack frame, the subtype field is set to 1101. Note: in Figure 3.7 and in most books, the fields are given in little-endian byte order, meaning that the least-significant bits are sent/written first. However, if you analyze network data, for example with network protocol analyzer, the frame will most likely be shown in big-endian format (also referred to as "network byte order"), where the most-significant bit is written first.

Duration

If a complete data frame or the final fragment of a fragmentation burst (in the case, that the data was fragmented into smaller pieces), the duration field is set to 0.

Receiver Address

The receiver address field is filled with the transmitter address of the frame being acknowledged.

The ack frame consists apart from the MAC header only of a subsequent frame check sequence (FCS), which allows the receiver to determine if the frame is flawed (see Figure 3.7).

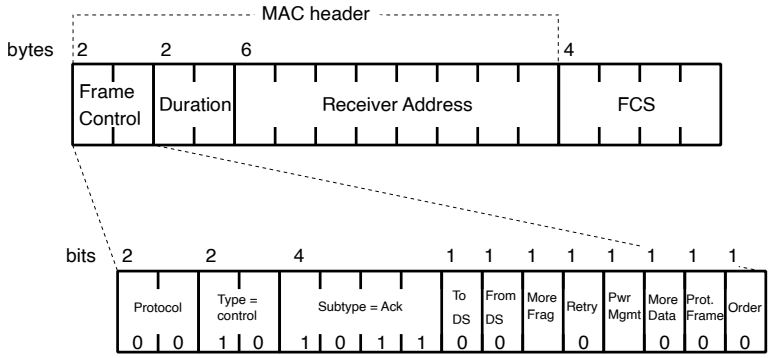

Figure 3.7: Acknowledgment frame structure

Null Frame

Since null frames play an essential role in the localization application, they are mentioned here. Null frames do not carry any data payload; they are solely used for power management information. In 802.11 networks, mobile stations use it to inform the access point (AP) about their power-saving status via setting the power management bit either to "1" one or "0" zero [16]. Zero indicates that the mobile station is online and ready to receive data. One indicates that the station is going into offline-mode. Therefore any frames that come into the AP for the station should be buffered. When the STA gets back online, it sends a null frame with the power management bit set to 1, and the AP starts forwarding the packets.

The overall structure is the same as the ack frame structure (compare with Figure Figure 3.7). It consists of the MAC header, followed by a four-byte long FCS field. For the null frame, the field type is set to data, 10 and the subtype value to 0100, which indicates that the frame is a null frame, and does not carry any data.

Null frames are further used in the localization application to trigger the device, which should be localized, to confirm the null frame's reception with an ack frame. A range estimation can be done knowing the round trip time between sending the null frame until the ack frame is received again.

4

Vehicle Wireless Channel Propagation

To be able to interpret measurement values from packet transmissions, it is vital to understand the effects on signals when transmitted over a wireless channel. When, like in the case of C-ITS, there is a relative movement between transmitter and receiver, a frequency shift, the so-called Doppler shift has to be taken into account. Also diffraction, reflections and scattering will alter the signal. The first part of this chapter addresses the propagation mechanisms of wireless channels, including the Doppler shift. The second part explains methods and considerations which have to be done in order to characterize a wireless channel stochastically.

4.1 Propagation Mechanisms

Transmissions over wireless channels present a challenge. Not only due to the interference through noise, nearby channels or because of transmitter/ receiver movement also processes like reflections, transmission, diffraction and scattering will alter the signal. This section will give a brief overview over these mechanism.

4.1.1 Path Loss

In the simplest case, the wireless transmission takes part between a transmit and a receive antenna in free space. In this particular case, the received power is a function of the distance. This can be explained as follows: Assuming an isotropic radiator, the transmit power P_{RX} is evenly radiated in all directions. Thus, around the radiator in a distance d, spheres with surface area $A = 4\pi d^2$ and power spectral density $S = P_{RX}/A$ are formed. The receive power P_{RX} at the receiver, using an antenna with effective area A_{RX} is then be given by:

$$P_{RX}(d) = P_{TX}\frac{A_{RX}}{4\pi d^2} \tag{4.1}$$

The effective area A_{RX}, also referred to as antenna aperture or receiving cross-section, is an antenna characteristic which describes how much power, in the perpendicular direction of an incoming planar wave is captured. For an isotropic antenna, with directivity $D = 1$, A_{RX} is calculated as [32]:

$$A_{RX} = \frac{\lambda^2}{4\pi} \tag{4.2}$$

Inserting (4.2) into (4.1) we get:

$$P_{RX}(d) = P_{TX}\left(\frac{\lambda}{4\pi d}\right)^2 \tag{4.3}$$

If the transmit antenna is non-isotropic, but has an antenna gain G_{TX} in the direction of the receiver, the receive power (4.3) becomes:

$$P_{RX}(d) = P_{TX}G_{RX}\left(\frac{\lambda}{4\pi d}\right)^2 \tag{4.4}$$

The gain G can be expressed in terms of the effective area A_e [32]:

$$G = A_e\frac{4\pi}{\lambda^2} \tag{4.5}$$

It is noticeable that assuming the effective area stays constant; the gain increases with higher frequencies.
When using a receive antenna with an effective aperture A_{RX} and a transmit antenna with gain G_{TX} in the direction of the receiver, using (4.5), the receive power can be written as:

$$P_{RX}(d) = P_{TX}G_{TX}G_{RX}\left(\frac{\lambda}{4\pi d}\right)^2 \tag{4.6}$$

This equation is also known as *Friis transmission formula.*

Friis transmission formula shows a fundamental fact in wireless transmission: Higher frequencies suffer from more attenuation. Or to put it another way, the path loss increases with frequency.

Sometimes it is convenient to calculate the path loss in decibels (dB). Therefore (4.6) can be written as:

$$P_{RX}|_{dB} = P_{TX}|_{dBm} + G_{TX}|_{dB} + G_{RX}|_{dB} + 20\log_{10}\left(\frac{\lambda}{4\pi d}\right) \tag{4.7}$$

Here, $|_{dB}$ and $|_{dBm}$ means that the value is given in the unit decibels respectively in decibels with reference to one *milliwatt*.
The transmission formula is restricted to deliver accurate results if the distance d, the so-called *Rayleigh distance*, between the transmit and receive antennas, is [15]:

$$d \geq \frac{2a^2}{\lambda} \tag{4.8}$$

where a is the largest linear dimension of either antenna.

4.1.2 Doppler effect and frequency dispersion

In the previous case, we assumed that the transmitter and receiver were stationary. But what happens if there is a movement between transmitter and receiver? Here, the received signal will have a frequency shift, known as *Doppler shift*. This is due to that the wave has to travel a longer or shorter distance Δd (see Figure 4.1) depending on the direction of movement. In the case, that the receiver drives away from the transmitter, the Doppler shift is given by:

$$f_d = -\frac{v}{\lambda}\cos\Theta \tag{4.9}$$

Where v is the speed of the receiver, λ the wavelength, calculated as $\frac{c_0}{f_c}$ and Θ the angle of arrival relative to the direction of motion [17]. Due to the changed travel distance, the receive signal phase is also shifted by:

$$\Delta\Phi = \frac{2\pi}{\lambda}\Delta d \tag{4.10}$$

Doppler shifts are generally in the range of 10 - 1000Hz. They only have a small impact on the transmission, e.g. the receiver can compensate the shift, however if there is more than one signal path with different frequency and phase shifts (i.e. in multipath environments) it comes to constructive or destructive interference which results in significant drops and fluctuations of the receive signal power over a small region. This fading is known as *small-scale fading / short-scale fading* or as *fast fading*.

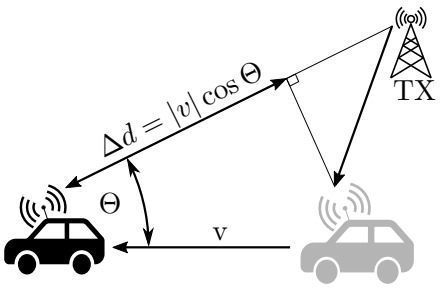

Figure 4.1: Doppler shift due to movement between RX and TX

4.1.3 Scatters

When signals are sent over wireless channels, the electromagnetic waves interact with dielectric and conducting objects. These interactions can be classified as:

- Reflection
  The reflection of waves determines the RX power at the receiver. Even in the simplest case, where no other scattering objects are around, the signals typically gets reflected by the ground.
- Transmission
  Especially if the transmitter or the receiver is behind a dielectric material, such as a windshield or a window in a car, the attenuation and the phase shift are of particular importance.
- Scattering
  In the case of rough surfaces, the incidental wave gets scattered which means, in addition to the specular reflection, multiple other reflections are introduced.
- Diffraction
  The effect of diffraction can be seen when waves bend around the corner of sharp edges.

The above-stated effects are generally summarized under the term *scatters*. Multiple scatters cause the transmit signal to travel via multiple paths. The receiver 'sees' different time-delayed copies of the transmit signal. Depending on the phase shift, the received signal can experience significant fades in the order of several magnitudes. In the following chapter section 4.2 focuses on the statistical description of wireless channels.

4.2 Statistical Description of Wireless Channels

To get a better understanding of how the received power varies, we take a closer look at Figure 4.2. It shows the received power plotted over the distance d between TX and RX on a

logarithmic scale. As it can bee seen; the received power is not only a monotonical function of the distance, it also varies widely. Generally, these variations are referred to as small scale and large scale fading introduced by multipath propagation. Before we focus on multipath fading, a few basic concepts about wireless channels are stated.

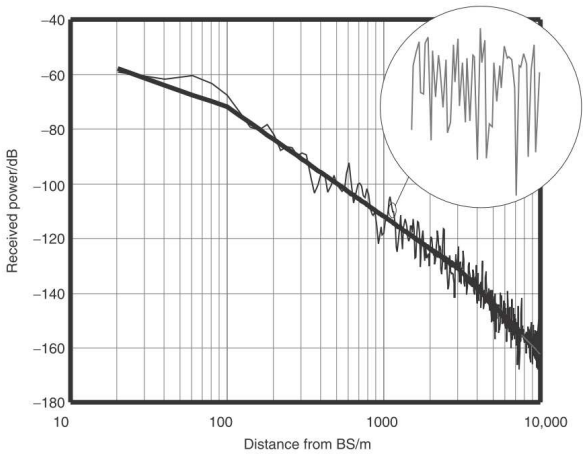

Figure 4.2: Typical receive power over distance (RX -TX) plot. Taken from [26]

Passband signals Any passbandsignal $s(t)$ can be written as:

$$s(t) = s_I(t)\cos(2\pi f_0 t) - s_Q(t)\sin(2\pi f_0 t) \tag{4.11}$$

where $s_I(t)$ is the in-phase component respectively $s_Q(t)$ the quadrature component and f_0 is a fixed frequency i.a. the carrier frequency

Delay spread τ Is the time, between the earliest arrival of a multipath component (mostly the LOS component)and the arrival of the last reflection; the inverse delay spread $1/\tau$ is called the *coherence bandwidth*

Coherence time T_c The coherence time states how long the channel impulse response stays constant; the inverse coherence time $1/T_c$ is called the *Doppler spread*

Linkage between delay spread and coherence time Depending on signal duration T and the delay spread, the channel is either called narrowband, which means that the frequency response is considered flat or if that is not the case, wideband. If the coherence time compared to the signal duration is relatively large, which implies that the amplitude and phase do not vary considerably during a period of transmission. If that is not the case, the fading is referred to as fast fading (cf. Figure 4.3).

Wide- sense stationarity (WSS) A random signal is called wide- sense stationary, if the mean and the autocorrelation function (ACF) A_s does not vary in time and is only a function of the time difference Δt.

$$A_s(\Delta t) = \mathbb{E}[s^*(t)s(t+\Delta t)] \tag{4.12}$$

where $\mathbb{E}$ is the expectation.

Uncorrelated scattering (US) If the autocorrelation function shows no correlation for different delays τ, we can assume uncorrelated scattering.

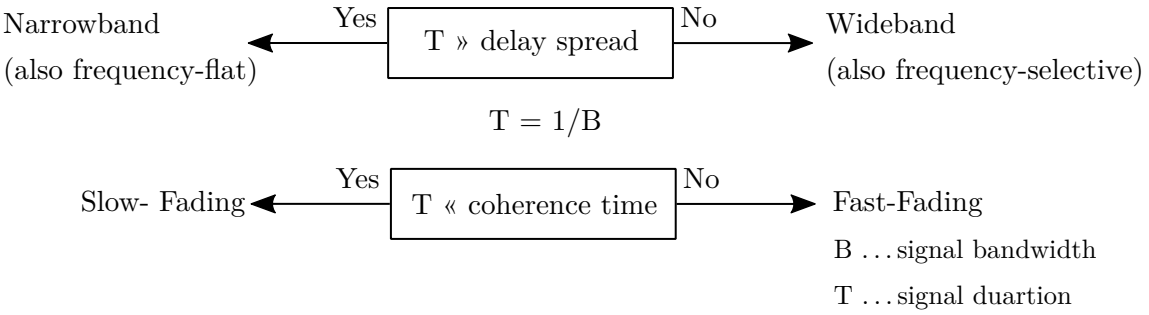

Figure 4.3: Linkage between delay spread and coherence bandwidth

Multipath fading

The main reasons for fading are shown in Figure 4.4. The effects can be roughly divided into two groups: Small scale and large scale fading. Small scale fading summarizes the power attenuation which happens when the receiver is moved on a scale of few wavelengths and are mainly to the different paths lengths and the Doppler shift. Large scale fading, however, describes the attenuation introduced by obstacles in the signal path.

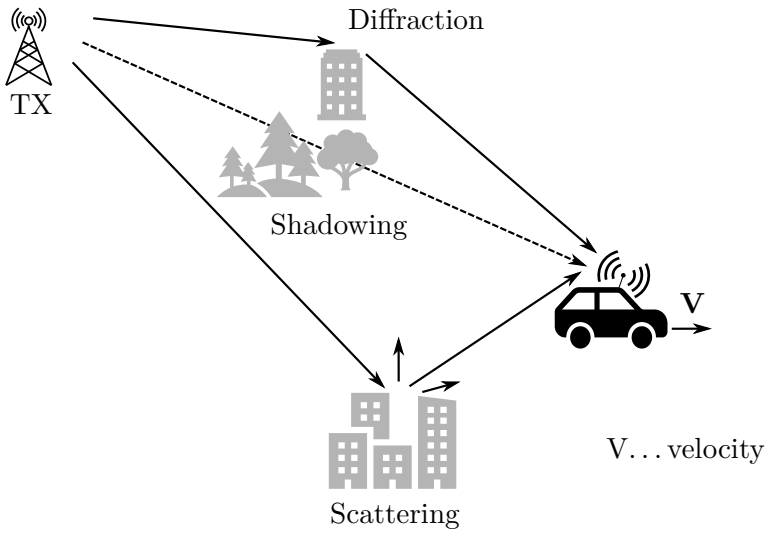

Figure 4.4: Multipath fading environment

Small Scale Fading

Small scale fading, also known as short scale fading, is the receive power variation, which manifests when the receiver or transmitter is moved by a few wavelengths. The signal may vary up to 30 to 40dB [18]. The reason for that is that each path has its Doppler shift (see Section 4.1.2), channel gain, and time delay introduced by the different path lengths. It can be shown (i.a. [17]), that even without knowing the exact probability density function (pdf) of each amplitude of the paths, we can give a pdf of the receive power.

The following assumptions are valid for narrowband channels.

Multipath propagation without a LOS path In the case, where there is no direct path and the individual signal phases are assumed to be uniformly distributed over the interval $[0, 2\pi]$ (see Figure 4.5), the pdf of r can be written as a *Rayleigh* distribution:

$$p_r(r) = \begin{cases} \frac{r}{\sigma^2} \cdot \exp(-\frac{r^2}{2\sigma^2}), & r \geq 0 \\ 0, & r < 0 \end{cases} \tag{4.13}$$

where σ^2 denotes the variance and r describes the magnitude of the complex valued field strength amplitude. It is assumed, that the receiver moves with constant velocity and the scatters around uniformly distributed around the receiving area.

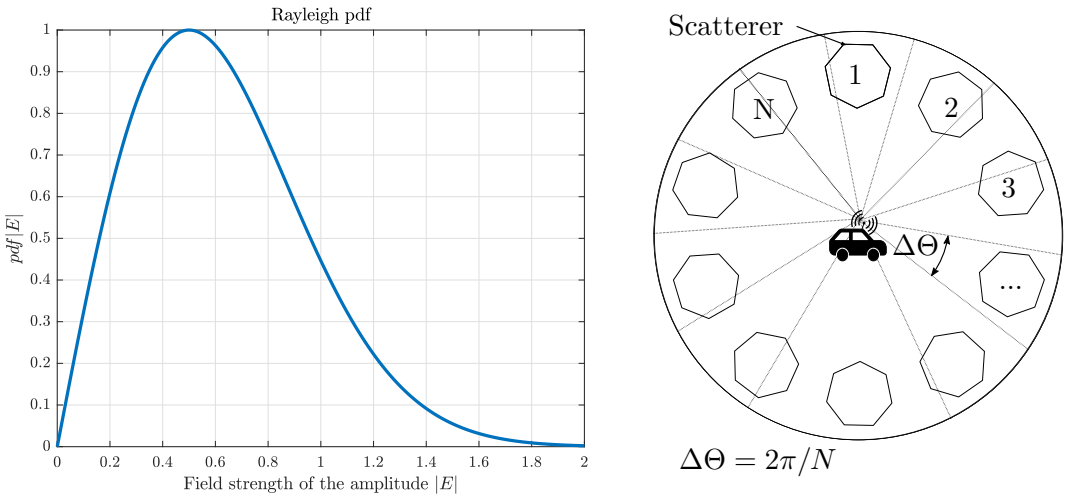

Figure 4.5: Multipath propagation without LOS path; Rayleigh distribution

Multipath propagation with a LOS path The considerations from section 4.2 remain the same but here, we have an additional LOS component which is assumed to be purely real with an amplitude A. The pdf of r is given by a *Rician* distribution ([30]):

$$p_r(r) = \begin{cases} \frac{r}{\sigma^2} \cdot \exp\left(\frac{-(r^2+A^2)}{2\sigma^2}\right) \cdot I_0\left(\frac{rA}{\sigma^2}\right), & r \geq 0 \\ 0, & r < 0 \end{cases} \tag{4.14}$$

where I_0 is the modified *Bessel* function of zeroth order. The term $K = A^2/2\sigma^2$ is called *Rice factor* K. $K = 0$ means that there is no LOS component and therefore a Rayleigh distributed receive power, $K = \infty$ describes a pure LOS communication without fading (Figure 4.6).

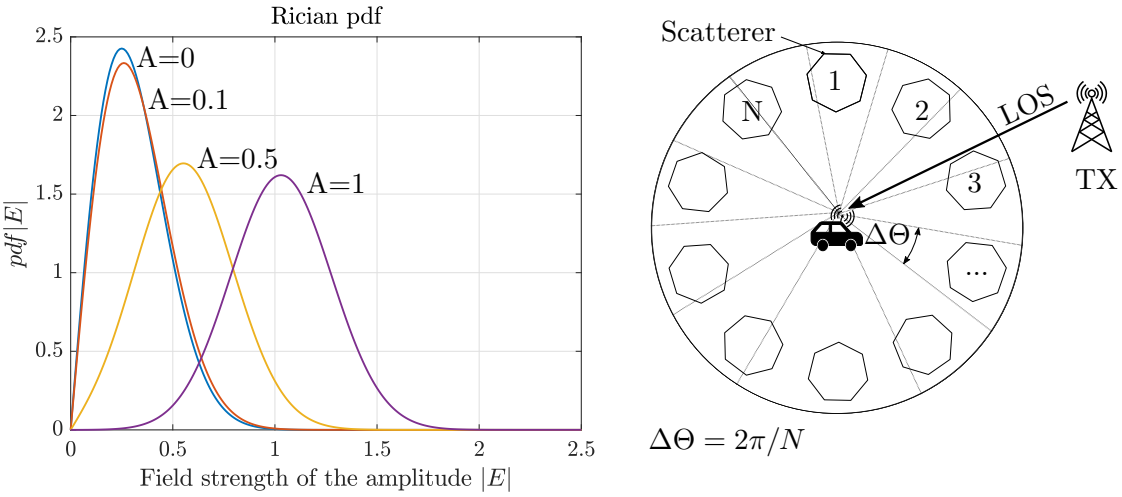

Figure 4.6: Multipath propagation with a LOS path; Rician distribution with different amplitudes A

Clarke's Model

To get an intuition of how fast the channel is varying, the model introduced by Clark [7] provides a useful tool. It assumes a uniform scattering environment, where each of the N multipath components has the same received power. The in-phase $r_I(t)$ and quadrature $r_Q(t)$ component of the receive power are assumed to be independent Gaussian processes, uncorrelated and WSS. If $N \to \infty$ and we take the ACF of the receive power $r(t)$ and eliminate the angle dependency via integrating over the interval $[0, 2\pi]$ we get (see Figure 4.7):

$$A_r(\Delta t) = P_r J_0(2\pi f_D \Delta t) \tag{4.15}$$

where P_r is the total received power and J_0 the Bessel function of zeroth order. To get the power spectral density (psd) $S_r(f)$ of the total receive power $r(t)$, we take the Fourier transform of the ACF (4.15):

$$S_r(f) = \begin{cases} \frac{P_r}{2\pi f_D} \frac{1}{\sqrt{1-(|f-f_C|/f_D)^2}}, & |f - f_C| \leq f_D \\ 0, & else \end{cases} \tag{4.16}$$

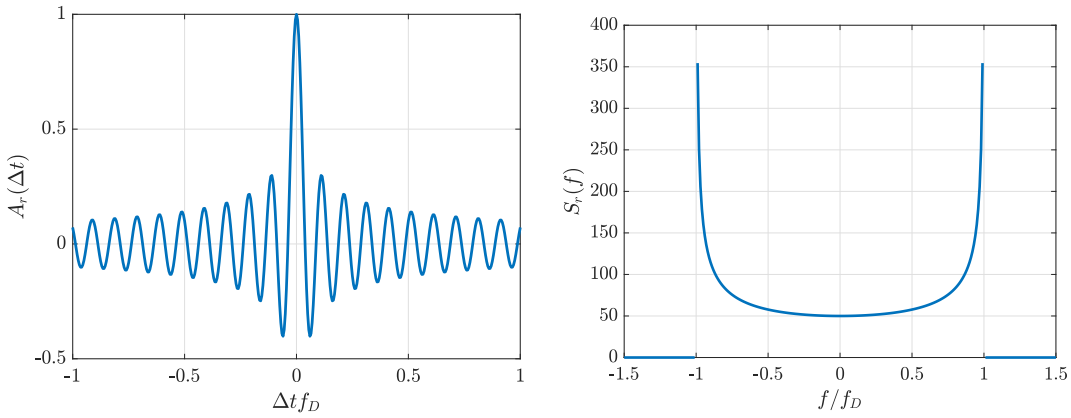

Figure 4.7: Left: Besselfunction Right: Jakes U-shaped spectrum

Large Scale Fading

Large scale fading manifests itself through the attenuation of the average receive power with respect to distance. It is mainly due to two processes: path loss, as explained in Section 4.1.1 and shadowing. Shadowing summarizes the signal attenuation, caused by large obstacles in the signal path such as buildings, hills, walls etc. Compared to small scale fading, large scale fading happens on a much slower timescale. An often used distribution to describe large scale fading is the **log- normal** distribution ([29]):

$$P_{RX}(d)|_{dB} = P_{TX}|_{dBm} - \overline{P_L}(d_0)|_{dB} + 10n \log\left(\frac{d}{d_0}\right) + X_\sigma|_{dB} \tag{4.17}$$

where P_{TX} is the transmit power, $\overline{P_L}(d_0)$ the average power at a reference distance d_0, n the path loss exponent which is normally somewhere between 1.5 for i.e. indoor LOS and 6 f.e. for shadowed urban cellular radios. X_σ is a zero-mean Gaussian distributed random variable with standard deviation σ. The values for n and *sigma* are in practice obtained from measured data.

5

Position Estimation Application

An essential step before actually implementing the position estimating algorithm was to make some preliminary examinations to understand the radio module's behavior, the distribution of the received signals, and limitations in use. Afterward, it could be simulated, based on the findings. The first section gives an overview of the application and states the results of preliminary considerations and measurements which were necessary before starting with the implementation. The second section describes the mathematics behind the application and presents briefly the MATLAB simulation used to point out possible difficulties beforehand. The last part describes the C implementation and goes into more detail regarding the realization.

5.1 Application description

This thesis's goal was to implement a position estimation algorithm on a roadside unit to augment the position estimation obtained from a conventional GNS system. The key aspect was to develop a low-cost solution that works with already existing hardware and could be employed by simply updating the software on the RSU. Which made it challenging was that there was no option to adapt or even figure out how the 802.11p radio module works on a low-level basis since it is sold as a ready-to-run component with limited configuration options.

5.1.1 Application overview

The application is based on the fact that in 802.11p, frames get acknowledged with an ack frame. The turnaround time needed to generate the ack response is called t_{SIFS}. It is defined as 32 µs. Therefore, if the RTT between the end of the data frame and start of receiving the ack frame is known, the pseudorange d can be calculated as:

$$d = \frac{c}{2} \cdot (RTT - t_{SIFS}) \tag{5.1}$$

where c denotes the propagation speed of the wave, further assumed to be the speed of light. Since this only gives a radius, where the to be localized target could be find in, at least two RSUs have to be used to get a position fix. As stated in Section 2.1.1, using two STAs, leads to two ambiguous solutions. There are different approaches to determine which of the solutions is the actual position. Some of them will be described further on.
In Figure 5.1, an overview of the application using two RSUs can be seen. Here, the RSUs send a null frame individually to the target, which replies with an ack frame. The RSUs receive the frame, capture the time, and send it to an evaluation unit, further referred to as Main Evaluation Unit (MEU), where the data is processed. To make this application as flexible as possible, the MEU is implemented as a module. The MEU can be employed either on an RSU or on an other Linux-based device such as a micro-controller, computer, or similar.

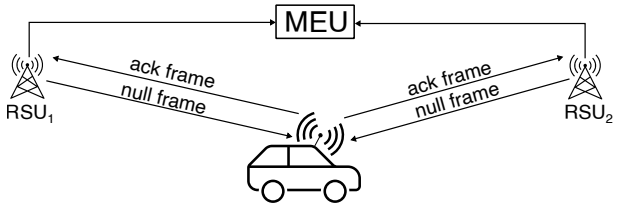

Figure 5.1: Application overview: both RSUs send independent from each other null frames, which are acknowledged by the target.

5.1.2 Preliminary Considerations

Before starting with the implementation, a few questions had to be answered:

- SIFS accuracy
  The entire application is based on the consistency of the turnaround time. Having a variant timing would make it impossible to estimate the position.

- Temperature dependency
  Since the radio module gives the RTT in ticks per 300 MHz, the oscillator-stability may be temperature-dependent, which would falsify the readings.

- Modulation and code rate dependency
  The application should work with different targets. That means the ack frame could be sent with different modulation schemes and rates. 802.11p does not specify which scheme and rate must be used for the ack frame.

- Correlation between RTT and transmit power
  A possible correlation between ack- transmit power and RTT could alter the results.

- Multipath effects
  Although OFDM based transmission schemes are robust against multipath propagation effects, a possible influence on the estimation accuracy should be determined beforehand.

SIFS Accuracy

Having a consistent turnaround time is vital in the proposed approach. Assuming a 10 MHz channel, the *SIFS* is defined as 32 µs with a tolerance of ±10 %, which calculates to 30.07 µs – 33.3 µs equally to an estimation error in the range of −195 m to 195 m. Two different IEEE 802.11p radio chipsets were tested regarding their SIFS accuracy. A software defined radio (SDR), as used in the Kapsch RIS-9160 RSU and their OBU CBX-9160, and a silicon chip installed on Kapsch's Localization Transceiver (LRX). For both tests, the devices were put next to each other to measure the SIFS. To isolate the devices from crosstalk of nearby channels and suppress effects of multipath propagation as far as possible, the devices under test (DUT) were put in a box with walls covered with Radiation-Absorbent Material (RAM). The transmitter, a Kapsch RIS-9160 RSU was configured to send 4000 packets, at a packet rate of 100 packets per second, on channel 178 (5.89 GHz). An LRX and a second RSU-9160 generated the ack frames. The ack-transmit power was set to 20 dBm, using a BPSK modulation scheme and code rate of 1/2.
The histogram in Figure 5.2 shows the distribution of the measured SIFS time. The left curve is obtained from the measurements with the RSU as ack-generator. It shows a bell-shaped distribution with a peak at 32 µs and a standard deviation of 13.8 ns. On the right side, the distribution is bimodal with peaks at 32.1265 µs and 32.175 µs. Repeating the measurements on different channels and different power levels yielded to the same results. In the following, the device which does the localization and sends the data frame is referred to as localization RSU, the ack-generating device as on board unit (OBU). It should be noted, that the referred OBU can be any IEEE 802.11p capable device which produces an ack frame.

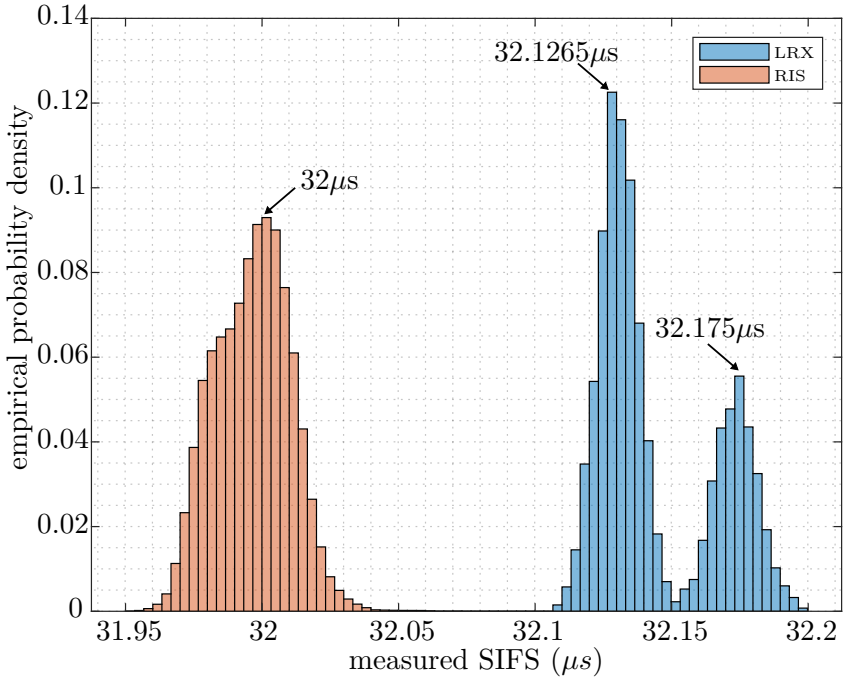

Figure 5.2: Histogram of the SIFS distribution from two different IEEE 802.11p radio modules.

Because of the bimodal shaped distribution, obtained from the silicon-based radio module, these modules are not suitable for the position estimation application.

Temperature Dependency

The RTT readings are given in ticks per 300 MHz which calculates to a maximum resolution of 0.5 m. This quantity is derived from the local oscillator in the radio module.
The oscillator is used for driving the SDR, rather than generating high frequencies for data transmission. Therefore, it is not designed to be highly temperature-stable, which leads to a slight frequency variation with changing temperatures. Tests showed that this only affects the ack-receiving side. The time (SIFS) needed to generate the ack stays constant over temperature changes. Since the position estimation accuracy should not be temperature-dependent, one of the preliminary considerations was to determine to which extent the radio temperature influences the measurements. Figure 5.3 shows the estimation error (EE) at different radio temperatures. The estimation error is calculated as:

$$EE = \frac{c}{2} \cdot (RTT - t_{SIFS}) - d_{act}, \tag{5.2}$$

where d_{act} is the actual distance, measured in meters. Since in this measurement both devices are placed next to each other, $d_{act} = 0$.

For each test, 2000 packets with a rate of 100 packets per second on channel 178 and a transmit power of 20 dBm, BPSK modulated and code rate of 1/2, were sent. Both devices were put in the measurement box, described in Section 5.1.2. The localization RSU temperature was measured using the built-in sensors, before and after the test. On average, the temperature increased by 1.5 °C. The distribution, seen on the left in Figure 5.3, was obtained by cooling the radio module down to 25 °C. The peak is still at 32 µs, which is equal to an estimation error of 0 m, but the overall distribution is slightly left-skewed. Bringing the radio module to normal operating temperature, which is in the range of 49 °C, leads to a bell-shaped distribution, with, again, a peak at 0 m. Further heating the module did not lead to a significant change.

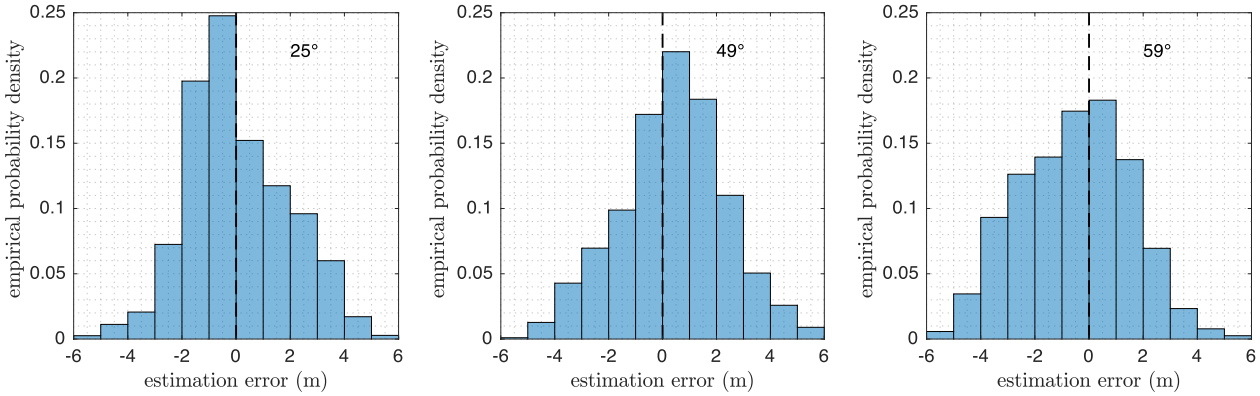

Figure 5.3: Estimation error at different radio temperatures; left: 25 °C, middle: 49 °C, right: 59 °C.

In summary, it can be said that the temperature does not noticeably change the estimations.

Modulation Scheme and Code Rate Dependency

Another influence factor which had to be checked before starting with the implementation was the modulation and coding scheme (MSC) dependency. Whether in the IEEE 802.11p standard neither in the radio module's datasheet was mentioned how the actual acknowledge frame is modulated. This had to be measured using the radio's built-in analyzing tool. The results are shown in Table 5.1.

The acknowledgment frame's modulation scheme is always the same as the modulation scheme of the sent frame. The ack code rate, however, is always 1/2, except if the sent frame is modulated with a QAM64 modulation, then the code rate of the ack frame is 2/3. Various MCS measurements with different MCS have been done to check for a dependency between MCS and RTT, but no correlation could be found.

TX Modulation scheme	Code rate		Ack Modulation scheme	Code rate
BPSK	1/2	→	BPSK	1/2
BPSK	3/4	→	BPSK	1/2
QPSK	1/2	→	QPSK	1/2
QPSK	3/4	→	QPSK	1/2
QAM16	1/2	→	QAM16	1/2
QAM16	3/4	→	QAM16	1/2
QAM64	2/3	→	QAM64	2/3
QAM64	3/4	→	QAM64	2/3

Table 5.1: TX modulation and coding scheme witch corresponding ack reply.

Correlation between RTT and transmit power

During the first tests, there were indications that the ack-transmit power and the RTT are correlated. More measurements have been taken to investigate this behavior further. A high correlation between transmit power and RTT would be a knock-out criterion for the proposed approach. In Figure 5.4 the RTT dependence of the RSS indication is shown. For the measurement, overall 17 000 packets, with a packet rate of 100 packets per second on channel 178 were sent. The data frames and the ack frames were modulated using a BPSK scheme, with code rate 1/2. The ack-transmit power was gradually increased, starting from 0 dBm to 20 dBm in 2.5 dBm steps. The devices were placed in a hallway, 5 m apart with direct line-of-sight (LOS). Two omnidirectional antennas, with an antenna gain of 6 dBi were used.

On the left vertical axis, shown in Figure 5.4, the RTT in microseconds is given; on the right vertical axis, the RSSI, in *dBm*, measured at the localization RSU side, is shown. The dotted line indicates the mean RTT, which is 32.033 µs. Subtracting the SIFS, and multiplying by the speed of light divided by two, calculates to 5 m. The RTT readings were smoothed using a moving average filter with a span of 50 for easier readability. As it can visually be seen, there is no coherence between RSSI and RTT. Calculating the Pearson correlation coefficient (~ 0.01) confirmed this.

For the previous measurements, the transmission power was set to be in the optimum operating range, far away from the receive sensitivity limit, at −90 dBm. To understand how the radio module handles low RSS values, a variable attenuator was placed in the localization RSU's receive path. MCS, distance, and packet rate remained unchanged, transmit power P_{RX} was reduced to 10 dBm. A directive antenna with a gain $G_{RX} = 14$ dBi and 6 m long connector cables, with an attenuation of 2.4 dB, were used on the receive side. The propagation delay of

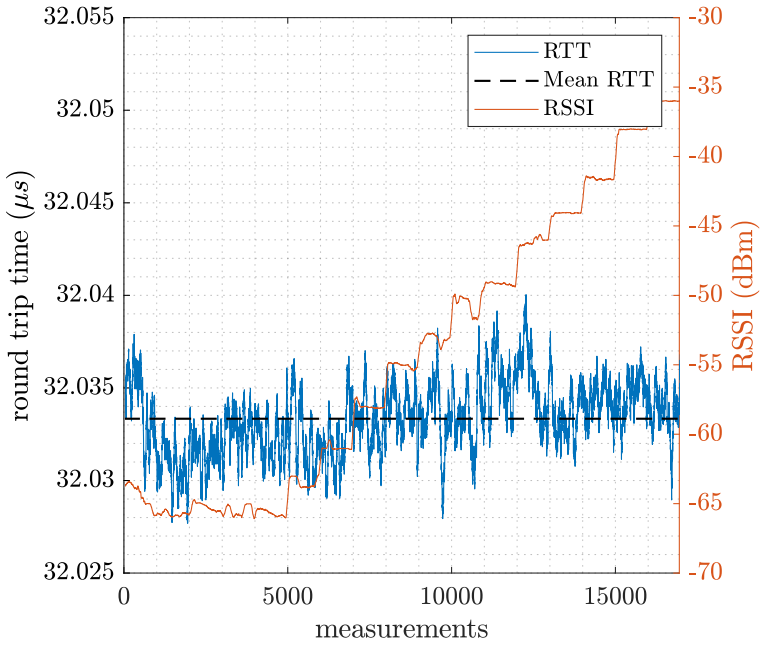

Figure 5.4: RTT versus RSSI

the cables was calculated and further subtracted from the measurements, as follows:

$$Delay = \frac{2d_{Cable}}{c \cdot NVP} \tag{5.3}$$

where d_{Cable} is the cable length. NVP is the Nominal Velocity of Propagation, a factor describing the percentage of light's speed that the signal travels down the cable. For the used 50 Ω cable, the NVP is given as 69 %. In Figure 5.5, the measurements with low RSS values are shown. The receive power P_{RX} was not captured at this measurement, therefore it had to be calculated using (5.4):

$$P_{RX} = P_{TX} + G_{TX} + G_{RX} - 2.4\,\text{dB} - Att + 20\log_{10}\left(\frac{\lambda}{4\pi d}\right) \tag{5.4}$$

where $G_{TX} = 6\,\text{dBi}$ is the transmit antenna gain, Att the additional attenuation introduced by the variable attenuator, λ the signal- wavelength which is $\sim 50\,\text{mm}$. On the vertical axis, the estimation error is shown. It is calculated as the difference between the actual distance and the mean value of the measured pseudoranges.

As can be seen, there is a correlation between estimation accuracy and RSSI. For low values, starting at $\sim -80\,\text{dBm}$, the error significantly increases, making the approach not suitable for large distances. It should be noted that the measurement was taken inside; therefore, multipath effects could have influenced the results.

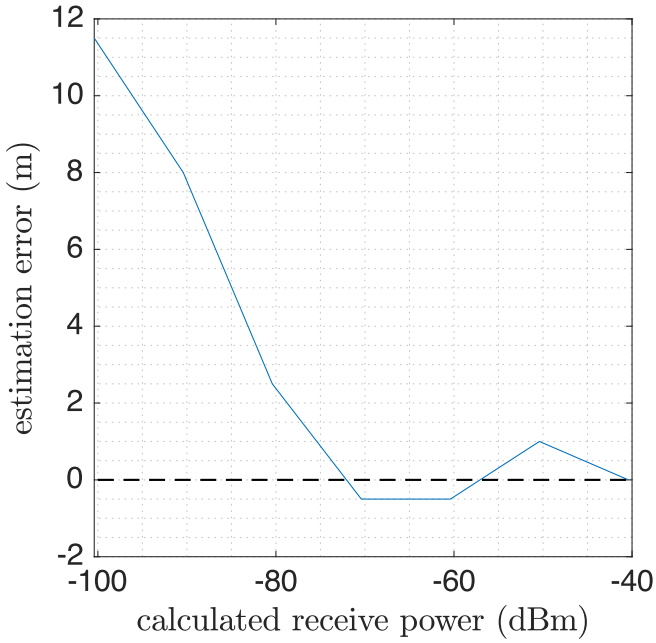

Figure 5.5: RTT versus low RSSI

Multipath effects

The proposed approach will mostly be used in surroundings where multipath effects are likely. Therefore, it is vital to understand where and to which extend these effects come into place and if they can be suppressed. Various measurements with different settings were taken. The following tests were done in a 2 m wide and 40 m long hallway, making it a perfect multipath environment. The walls were mostly made out of drywall with metal frames behind, and doors with a metal/glass frame. The influences can be seen in Figure 5.6. Transmit settings stayed the same. At each measurement point, 4000 packets were exchanged, on both sides were omnidirectional antennas with a gain of 6 dBi mounted. The position of the localization RSU remained unchanged, the counterpart station was moved along the hallway.

The horizontal axis in Figure 5.6 shows the displacement between both stations; the vertical axis represents the estimated distance; the dotted line indicates the desired value. The boxes' top and bottom indicate the 25th, respectively, the 75th percentiles of the pseudorange measurements at each point. The red horizontal bar within the box, the median, and the whiskers represent the most extreme data points. It can be seen that all estimated pseudoranges are far off the actual distances, which worsens with increasing distance. Which gets along with it, is an increase of the standard deviation, indicated by a larger range between the percentiles. Also noticeable, that the presence of metal/glass frames is directly visible, for example, at distances 10 m, 14 m and 20 m.

The estimation error distribution from the measurement at $d = 10\,\text{m}$, shows that there is not a single reading close to the actual distance. However, the distribution looks shape-wise, broadly

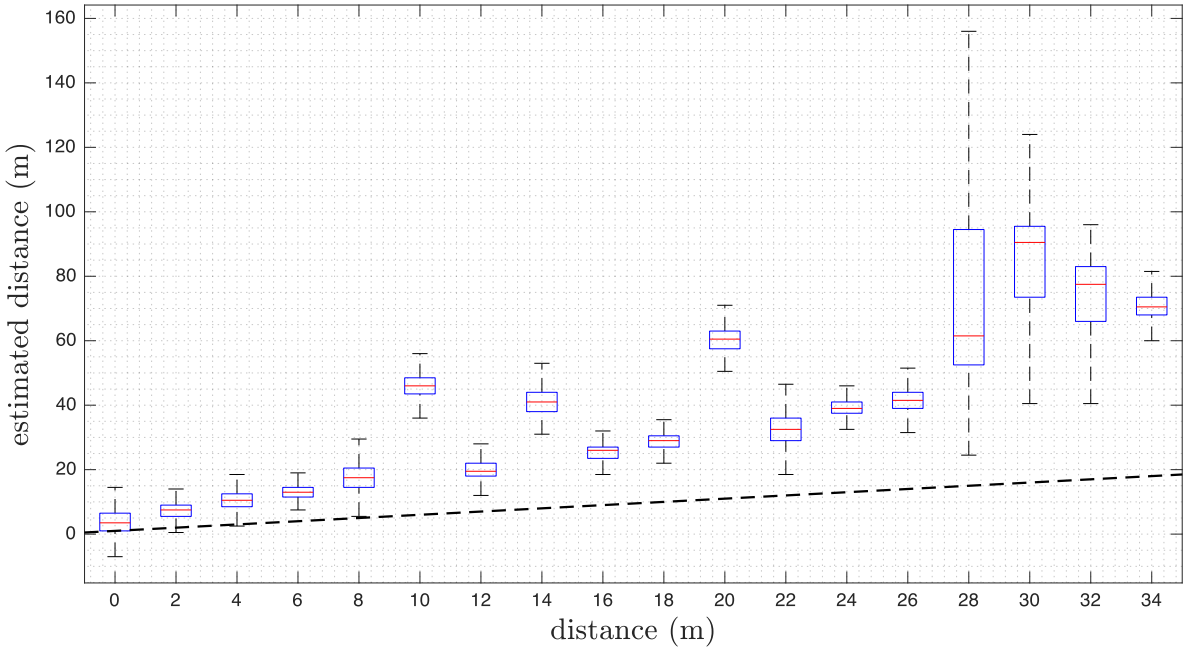

Figure 5.6: Boxplot of an indoor measurement with multipath propagation; the dotted line represents the expected measurement values.

similar to the ones measured inside the radio absorbent box. Repeating the measurements with different transmission parameters led to the same results.

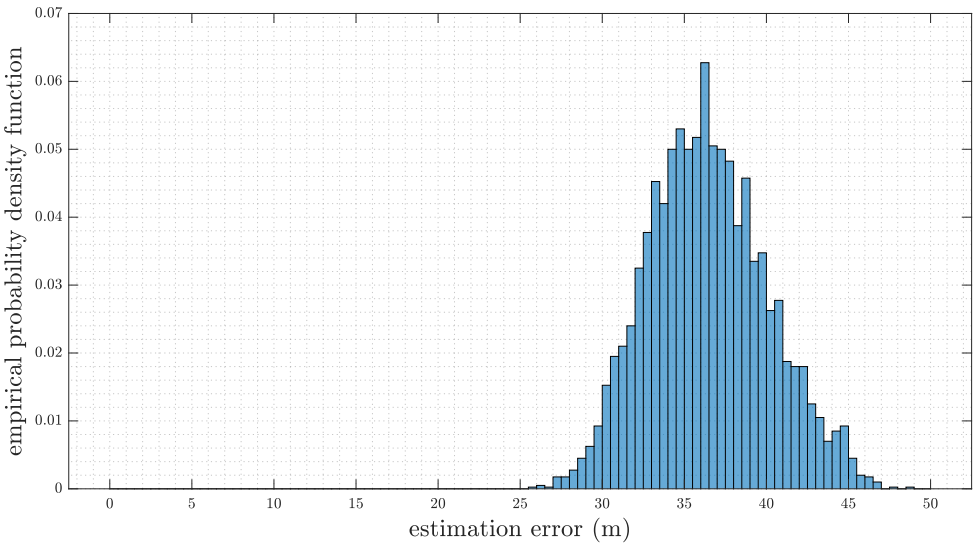

Figure 5.7: Estimation error distribution at a distance of 10 m. The shape of the measurement distribution looks as expected, but all measurements are shifted to higher values caused by multipath propagation effects.

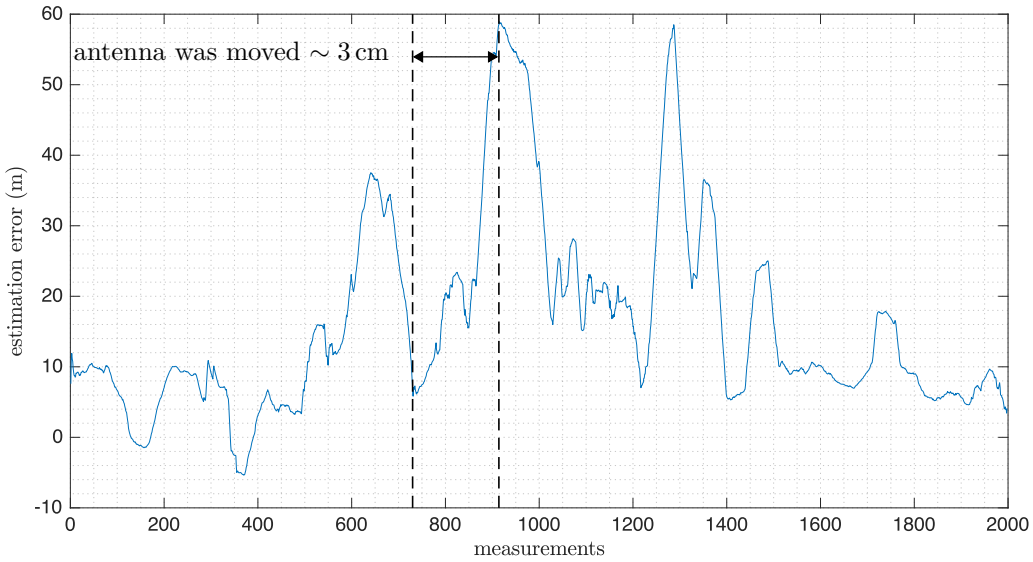

Figure 5.8: Effects of multipath propagation, receive antenna was moved by half a wavelength resulting in a destructive superposition of the signals causing an increase of estimation error.

Further investigations and measurements led to a highly probable explanation. For another test, the transmission parameters stayed unchanged. The devices were $d = 10\,\text{m}$ apart. Compared to preceding measurements, the antenna on the localization RSU was moved in the scope of centimeters. As shown in Figure 5.8, it can be seen that an antenna motion of $\sim 3\,\text{cm}$ let the estimation error drop from $-6\,\text{m}$ to $-60\,\text{m}$. A displacement of the antenna of $\sim 3\,\text{cm}$ equals roughly half of the wavelength, which is $\lambda \approx 5\,\text{cm}$. This may result in a destructive superposition of the received signal, which is a typical indication of small-scale fading. The first decodable signal may already have been reflected multiple times, resulting in several meters' estimation error. Yet, repeating these measurements outdoors with less multipath effects showed near-perfect measurement results with estimation errors in the range $\pm 1\,\text{m}$. In summary, it can be said that multipath effects and low RSSI can massively alter the pseudorange estimations. However, temperature and MCS do not have an influence.

5.2 Application Simulation

Before the implementation was tested in a real-world setup, simulations were used to analyze several setups and scenarios. Setups with two RSUs have been simulated as well as setups with three. Cost considerations and convenience requirements for a real-world deployment resulted in a compromise setup with only two localization units at a limited loss in accuracy.

5.2.1 Mathematical Computations

The application is based on computing the intersecting points of two circles in the plane. In general, two circles may or may not intersect. If they intersect, they will likely intersect in two points, not just one. This shows that additional information is needed to ensure a unique solution to the localization problem. In this project, there was no heading information available from any Inertial Navigation System (INS), nor the GNSS coordinates from the OBU. For this reason, the application tracks the target over a continuous period in time and determines the RSU to which the target is moving. Using the past history of the targets trajectory aids in removing ambiguity of the solution. Theoretically, two consecutive measurements would be sufficient for achieving a unique solution, but outliers in the acquired data need to be detected. Hence, the application tracks the target for at least ten seconds in time.

Circle- Circle Intersection

After converting the RTT measurements into pseudoranges, the intersecting points of two circles need to be determined. Two circles may intersect with each other in zero, one or two distinct points, cf. the illustration in Figure 5.9(a), (b), or (c).

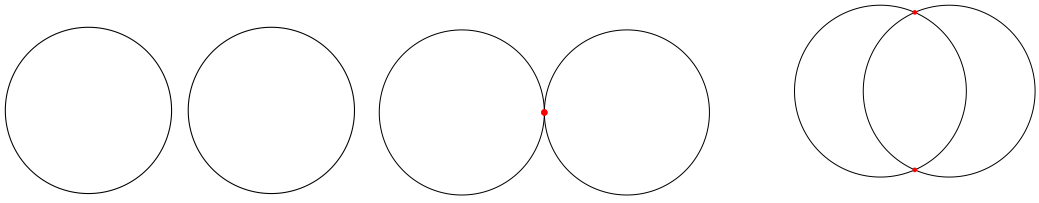

(a) No intersection (b) Intersect in a single point (c) Intersection in two distinct points

Figure 5.9: Circle- circle intersection

It turned out that using a geometrical approach for calculating the intersection points of two circles, as it is described in the following, is convenient to implement into C code and delivers accurate results.

Assuming two circles in the 2D plane, one centered at the origin at (x, y) with a radius r_1, the other one at (x_2, y_2) with $(x, y) \neq (x_2, y_2)$ and radius r_2, we got:

$$x^2 + y^2 = r_1^2 \tag{5.5}$$

$$(x - x_2)^2 + (y - y_2)^2 = r_2^2 \tag{5.6}$$

Subtracting Equation (5.5) from Equation (5.6) gets us:

$$x \cdot (-2x_2) + y \cdot (-2y_2) + (x_2^2 + y_2^2 + r_1^2 - r_2^2) = 0 \tag{5.7}$$

Comparing Equation (5.7) with a line given in line coordinates $Ax + Bx + C = 0$, we define:

$$A = -2x_2 \tag{5.8}$$

$$B = -2y_2 \tag{5.9}$$

$$C = x_2^2 + y_2^2 + r_1^2 - r_2^2 \tag{5.10}$$

This reduces the problem of finding the intersection points of two circles into finding the intersection between a circle and a line. The next step is to find the point (x_0, y_0) (cf. Figure 5.10), which is closest to the origin. The distance d_0 between (x_0, y_0) and the origin is calculated as:

$$d_0 = \frac{|C|}{\sqrt{A^2 + B^2}} \tag{5.11}$$

Since the vector (A, B) is perpendicular to the line intersecting the circle, the coordinates of the point (x_0, y_0) must be proportional to the coordinates of the vector (A, B). The distance from the origin to the point is already known, hence, we only have to scale the vector (A, B) as follows:

$$x_0 = -\frac{AC}{A^2 + B^2} \tag{5.12}$$

$$y_0 = -\frac{BC}{A^2 + B^2} \tag{5.13}$$

At this point, we can ascertain the number of intersection points. If d_0 is greater than the radius r_1, there are no intersection points. In the case that $d_0 = r_1$, there is exactly one intersection point. If $d_0 \leq r_1$, there are two intersection points; one at (a_x, a_y), and at (b_x, b_y). We know, they must be at the same distance d from (x_0, y_0) and also have to be on the line $Ax+Bx+C = 0$. Therefore, we first calculate the distance d as follows:

$$d = \sqrt{r_1^2 - \frac{C^2}{A^2 + B^2}} \tag{5.14}$$

From here, we only have to scale the vector, which is perpendicular to (A, B), namely $(-B, A)$, to the length d and add or subtract it to the point (x_0, y_0). The scaling factor, denoted as s, is obtained as:

$$s = \sqrt{\frac{d^2}{A^2 + B^2}} \tag{5.15}$$

Lastly, the equations for the intersection points (a_x, a_y) and (b_x, b_y) are:

$$a_x = x_0 + B \cdot s \tag{5.16}$$

$$a_y = y_0 - A \cdot s \tag{5.17}$$

$$b_x = x_0 - B \cdot s \tag{5.18}$$

$$b_y = y_0 + A \cdot s \tag{5.19}$$

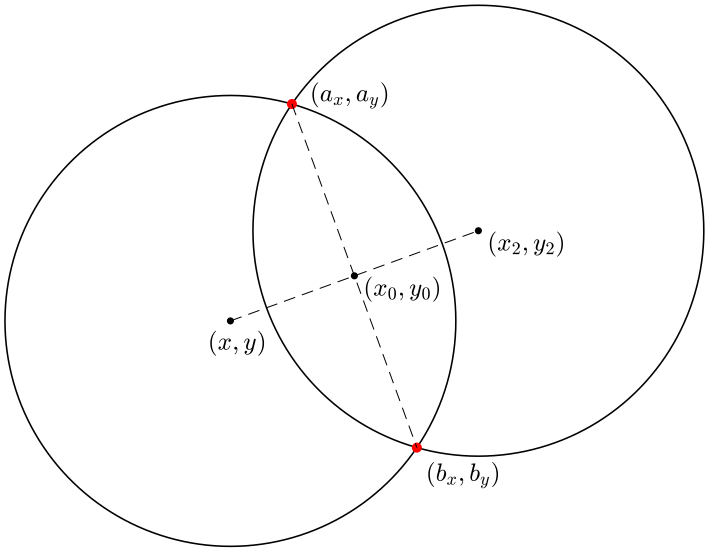

Figure 5.10: Circle - circle intersection calculation

Boundary Conditions

Depending on the RSU setup, one of the two solutions may lay outside of the road. In this case, the remaining one is the one we looked for. It also might be that the estimation is highly erroneous and is, thus, outside of the area one can expect the OBU to be. Defining boundary conditions enables to detect and discard these estimations. The boundaries are defined as lines, as shown in Figure 5.11. The blue line is further referred to as the eastbound, starting at (x_{east1}, y_{east1}) and ending at (x_{east2}, y_{east2}). The orange line on the left, is referred to as the westbound. It starts at (x_{west1}, y_{west1}) and ends at (x_{west2}, y_{west2}). Every estimation which is either left of the eastbound, respectively right from the westbound, is assessed as not valid. RSU_1, positioned at (x_{RSU1}, y_{RSU1}) constitutes the origin.

The following considerations are regarding the westbound; the calculations for the eastbound are vice versa. The boundary checks are based on the Hesse normal form, which is used to calculate the distance between the boundary and the estimation. First, we have to find the orthogonal vector $\vec{n}$, perpendicular to the boundary line. Having found that, the distance d,(cf. Figure 5.11) between boundary line and origin can be calculated as:

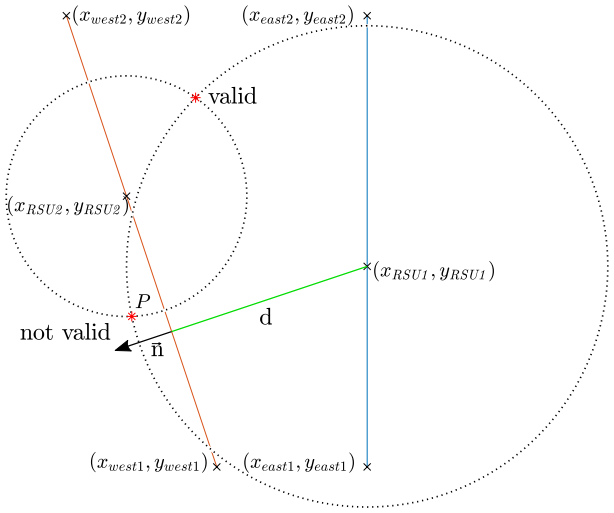

Figure 5.11: Outlier detection via boundary conditions

$$d = \vec{p} \cdot \vec{n_0} \tag{5.20}$$

where $\vec{p}$ denotes the support vector from the origin to the boundary line, $\vec{n_0} = \frac{\vec{n}}{|\vec{n}|}$, the normalized vector $\vec{n}$ and $\cdot$ the inner product. In the next step, the distance $d(P, g)$ from the estimation point P to the boundary line g has to be determined. Thereto, the Hesse normal form can be used as:

$$d(P, g) = \vec{q} \cdot \vec{n_0} - d \tag{5.21}$$

where, $\vec{q}$ denotes the position vector of P. Assuming, we evaluate the validity of point P, shown in Figure 5.11, in regards to the west boundary, $d(P, g) \leq 0$ must apply. Since this is not the case, the estimation P would be discarded.

Latitude and Longitude Conversion

So far, the calculations have been based on the 2D coordinate system in which RSU_1 represents the origin. Before outputting the estimations, they have to be converted into a Geographic Coordinate System (GCS), where positions on the earth's surface are given in latitude and longitude, as seen Figure 5.12a. The latitude ϕ, abbreviated as lat, describes the angle between the equatorial plane and a straight line perpendicular to it, which passes through the earth's center. The longitude λ, abbreviated as long, is the angle, either east or west of a reference meridian. Each meridian starts or ends at the North, respectively South pole. The first step from the coordinate transformation is to convert the Cartesian coordinates estimations to lat/long coordinates. Here, the azimuth angle γ, shown in Figure 5.12b, which describes the rotation between North and the reference x-axis, must be determined.

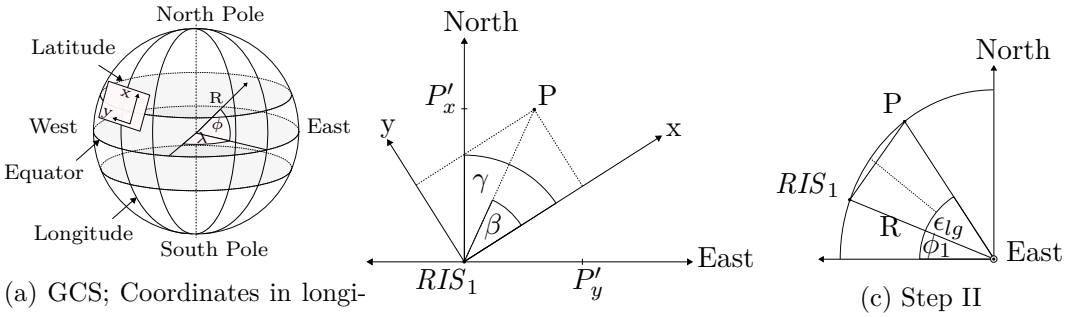

(a) GCS; Coordinates in longitude and latitude.

(b) Step I

(c) Step II

Figure 5.12: Coordinate transformation from reference system to CGS.

In the next step, the estimation P is projected onto the North- and East -axis. This can be done, assuming that the estimations distances compared to the earth curvature are relatively small, and the considered section is assumed to be flat (shown in Figure 5.12b). Finally, the lat and long angle difference ϵ_{lt} and ϵ_{lg}, between RSU_1 and P can be calculated. For the longitude difference ϵ_{lg} as:

$$\epsilon_{lg} = 2 \arcsin\left(\frac{|P|}{2R \cdot \cos(\phi_1)}\right) \cdot \sin(\gamma - \beta) \tag{5.22}$$

where $|P|$ denotes the distance between the origin in the reference coordinate system and the point P. β is the angle between P and the reference x-axis, ϕ_1 the latitude position from RIS_1 and $R = R(\phi)$ the radius of the earth. Because the earth is not perfectly round, a spheroid (ellipsoid of revolution) model is often used to approximate the earth's shape. The radius at an altitude Alt is calculated as:

$$R(\phi) = \sqrt{\frac{\left(R_1^2 \cdot \cos(\phi)\right)^2 + \left(R_2^2 \cdot \sin(\phi)\right)^2}{\left(R_1 \cdot \cos(\phi)\right)^2 + \left(R_2 \cdot \sin(\phi)\right)^2}} + Alt \tag{5.23}$$

where $R_1 = 6378.137\,\text{km}$, which denotes the equator radius at sea-level and $R_2 = 6356.752\,\text{km}$ the radius at the poles. The latitudinal angle difference ϵ_{lt} is calculated as:

$$\epsilon_{lg} = 2 \arcsin\left(\frac{|P|}{2R}\right) \cdot \cos(\gamma - \beta) \tag{5.24}$$

The last step is to add the angle differences to the RSU_1 coordinates, positioned at (ϕ_1, λ_1). The position estimation P is then at $(\phi_1 + \epsilon_{lt}, \lambda_1 + \epsilon_{lg})$.

5.2.2 Simulation

Using MATLAB allows to analyze several setups and scenarios without needing comprehensive real-world measurement data. Using a bootstrapping method allowed to model real- world RTT distributions while having only a small dataset available. Here, the set of data is sampled multiple times, and each time, in this case, the variance and the median is calculated. Subsequently,

the distribution is determined based on the individual median and variances. The following parameters can be adjusted:

- Timing offset
  In real operation, the transmission of the null frames will not happen perfectly simultaneously. This timing offset can be set.
- Variance and mean
  In order to simulate different types of measurement environments, the distribution, mean and variance of the pseudoranges can be adjusted.
- RSU geometries
  The position of the RSUs relative to each other defines the position of the ambiguous solutions obtained via the circle- circle intersection. If the setup is chosen correctly, the second, unwanted solution will violate the boundary condition and be discarded, resulting in a unique solution without needing further information.
- Boundary conditions
  As described in Section 5.2.1, the boundary conditions can be set and adjusted.
- Velocity of the tracked device
- Filtering and smoothing
  Basic filtering and smoothing algorithms, such as a moving average filter are implemented.

In Figure 5.13, a passing maneuver using MATLAB simulation is shown. On the left side, the setup up can be seen. The RSUs are diagonally placed on either side of the road. A car, represented by a black rectangular placed at $\sim 30\,\mathrm{m}$, should be overtaken. The blue circles depict the ideal position estimations. It can be seen that the car slows down before passing and accelerates afterward, indicated by the increased distance of the circles. In Figure 5.13b, the simulated estimation is shown. The black dots indicate the first, the blue dots, the second solution of the intersection points. The individual points are averaged using a moving average filter with a span of eight samples. The target device passes through the 60 m section in 33 s, which calculates to a rather moderate cruising speed of $1.81\,\mathrm{m\,s^{-1}}$. The RSUs sample the target position every second. It is assumed that the pseudorange estimations are Gaussian distributed, with a mean error of 2.1 m and unit variance. These values reflect typical measurement errors in near multipath-free environments. It is noticeable that towards the end of the section, the two circles intersect in a flat-angle, resulting in a deterioration of the estimation accuracy.

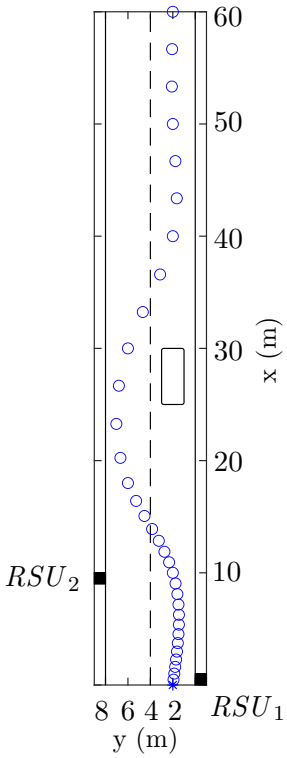

(a) Estimation setup; the black filled boxes represent the RSUs. The rectangle at ~ 30 m represents a car that should be passed. The blue circles indicate the position of the OBU.

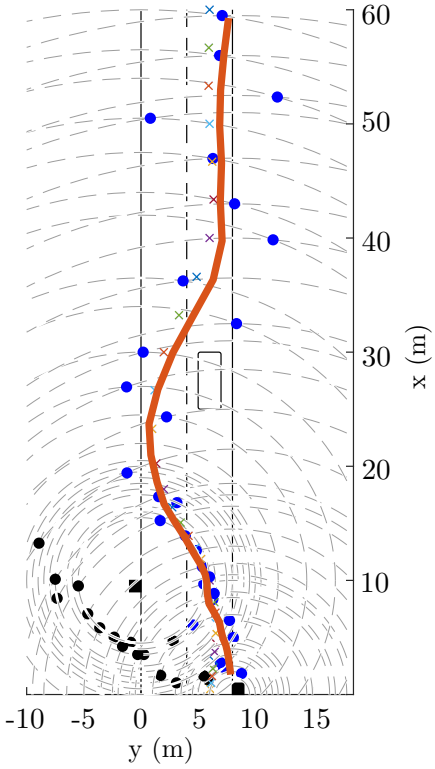

(b) Calculated position estimation; the black and blue dots represent the two solutions of the circle-circle intersection; the orange line is the estimation trajectory of the OBU obtained via averaging the position estimations with a moving average filter.

Figure 5.13: Example of a position estimation procedure using MATLAB.

5.3 Implementation

After thoroughly examining the radio module's behavior at different settings, measurement environments, implementing the algorithms in C language was the next step. Particular emphasis was laid on a modular design, allowing the use of three or more RSUs without changing the code and simultaneously keeping the impact of the localization application as small as possible since the main functionality of the RSU should not be disturbed. The main evaluation unit should be deployable either directly on one of the participating localization RSUs or on an external, Linux-based device. An overview of the application architecture is shown in Figure 5.14.

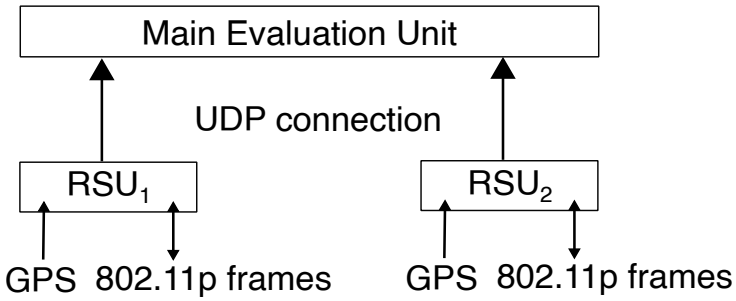

Figure 5.14: Overview of the application using two localization RSUs. Each RSU has a built-in GPS receiver module and an 802.11p radio. Synchronization among themselves is not required. Both units send their data via a UDP connection to the MEU for further processing.

Both RSUs work independently from each other, and therefore do not need to be connected or synchronized. Each of them is equipped with an 802.11p radio module and a GPS receiver. The GPS signal is only used for the Pulse Per Second (PPS) signal, which allows for accurate timing synchronization.
The RTT readings are sent via a User Data Protocol (UDP) connection to the MEU, where they are further processed. The data can be sent over WLAN or via an Ethernet connection. In the following, the localization RSU and the MEU are presented.

5.3.1 Localization RSU Implementation

Each RSU sends a null frame to a target device, which acknowledges the reception with an ack frame. Knowing the RTT of this procedure, the pseudorange can be calculated. If the RTTs of two different RSUs are combined, a position in the 2D plane can be estimated.
However, the default RSU runs a standard ITS-G5 communication architecture as it is defined for ITS stations in [9] and shown on the left side in Figure 5.15. Yet, ITS is based on broadcast messages and therefore the ability of sending unicast messages is not foreseen. Consequently, the first step was to implement a null frame-send method which allows to send a frame to a single MAC address. Furthermore, to localize a target, it has to be detected first. Therefore, the Access Layer (AL) of the RSU was adapted. Thus, the receive function, which is called, when the radio module receives a message, was modified to pass the information on, to where the localization implementation is able to further process it.
The receive function differentiates between two types of messages: receive and transmit-event packages. The former, receive packages are in general broadcast messages from other ITS users, which contain the looked for source MAC address. In general, ITS stations send broadcast messages, or beacons, every couple of seconds. The latter, transmit-event messages, are created by the radio and indicate that a previously sent message was successfully received. These messages contain the RTT, destination MAC address, and a timestamp.
If a message is received, the modified receive function calls a callback, implemented in the lo-

calization part of the program, and passes the information. The callback pushes the info onto a buffer, to prevent blocking from the AL. Therefore, the performance impact on the AL is kept to a minimum.

At the localization part, the data is pulled from the buffer, and a unique hash key is calculated from the MAC address. Further on, the address, RTT, and a timestamp from when the message was received are stored in a hash table with a fixed size N. If the source MAC address respectively the key, is new or unknown yet, the address is stored in an empty slot. The position of this slot is determined by the calculated hash key. If the MAC address is known, the RTT and the timestamp to the corresponding address are updated. This process is done in a thread, referred to as "Thread I" (cf.Figure 5.15). It continuously updates the entries and deletes old ones.

A second thread, "Thread II", iterates through the complete hash table according to an iteration schedule which is calculated at the startup. Assuming that the hash table has N entries, the overall iteration time, of one second, is divided into $N + 1$ parts. The first slot starts at zero. The second one, at $1/(N + 1)$ seconds and so forth. The last slot starts at $N/(N + 1)$ seconds. The iteration process continuously starts at every full second. If the first slot is not empty, a null frame is sent to the MAC address, stored there, and subsequently slept precisely until the next time window starts. If the first slot is empty, it is slept until the next time slot begins. The last slot is reserved for sending the RTT readings via UDP to the MEU.

This method allows several RSUs to send null frames to a target device within a time offset in the range of sub-milliseconds without the need for a direct synchronization among themselves. This scheme also allows to add additional RSUs to the localization process. Changes only have to be made on the MEU side.

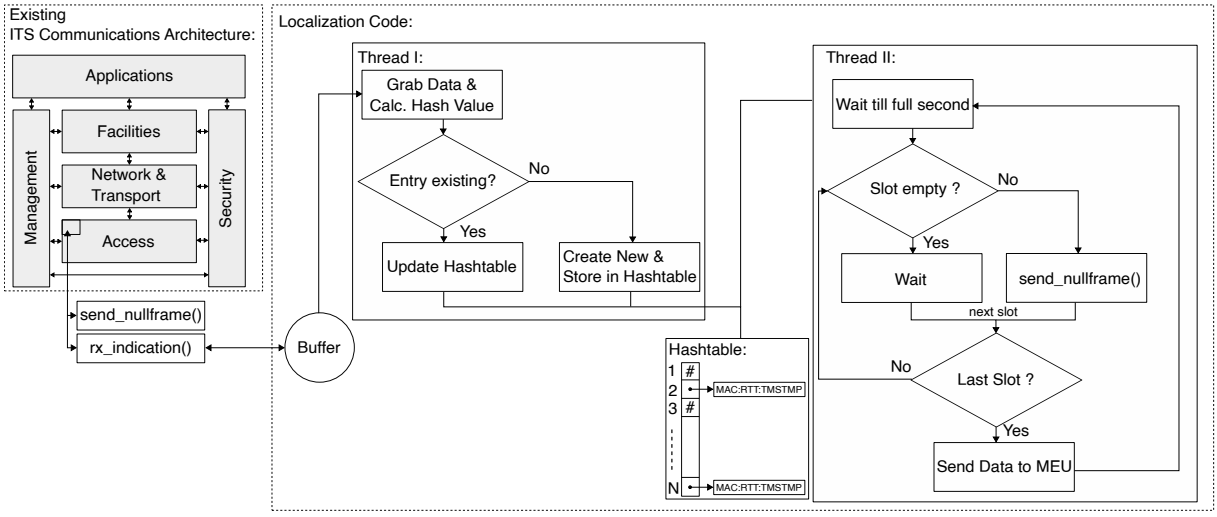

Figure 5.15: Flowchart of the RSU implementation; the left side shows the already existing ITS communication architecture with the modifications to the access layer. The middle and right side shows the newly implemented code.

5.3.2 Main Evaluation Unit Implementation

The main evaluation unit implementation is relatively straightforward. The MEU creates a UDP socket, binds the socket to the server address, and waits for datagram packets from the localization RSUs to arrive. These packets contain the RSU and the target MAC address, a receive timestamp, and the RTT. After matching the localization information obtained from two RSUs corresponding to a single OBU, the values are stored in a hash table.

Particular attention was paid that the offset between corresponding RTT values is not larger than 20 milliseconds; otherwise they will be discarded. This value was arbitrarily chosen based on the assumption that a tracked car's maximum speed is less than $50\,\mathrm{m\,s^{-1}}$. In this case, a timing offset of 20 milliseconds would mean that one of the units measured the target at a position 1 m apart from where the other unit measured it. Assuming that the timing offset is in a reasonable range, the position is calculated as stated in Section 5.2.1. Additionally, a moving average filter was implemented which helps to smooth the acquired position estimations.

If the environment is prone to multipath propagation, the application can switch to a more robust one-dimensional estimation. Here, the target is projected to the middle of the street and only the position lengthwise will be given.

The parameters, such as the position information of the participating RSUs, boundary conditions, rotation of the reference coordinate system to North and the logging level, is given in a configuration file, which will be read at startup. A callback registration function is implemented to allow external applications to have access to the position estimation. Further data processing such as Kalman- or maximum likelihood estimation was planned, but not implemented. It turned out that strong multipath effects affect the measurements to the extent that the implementation does not deliver useful estimations at all. Even additional processing would not help.

6

Measurements

This chapter presents selected measurement series taken outdoors. In the first section, an one-dimensional pseudorange estimation is shown. This measurement was a critical point. Based on it, the decision was made, that a position estimation using the RTT of the ack frame is doable. In the following sections, test results of the implemented application are presented. The problems are highlighted, and improvements, which were further on implemented and tested in subsequent measurement campaigns, are stated.

6.1 Pseudorange measurements

Before starting with the implementation, various measurements have been taken using a modified version of the RSU built-in analyzing tool, which allowed storing the measurement values to further process and analyze it. An essential question was if the estimation accuracy in an outdoor environment is high enough to allow for a position estimation within the range of a few meters. Thereto, a measurement series was taken on the testing ground of the ÖAMTC driving technique center in Teesdorf/Lower Austria. Two RSUs, one acting as the localization unit, the other one as ack generator, were placed along a line. After each measurement, which involved the transmission on 2000 packets, the distance was increased and measured again. Transmit power of the localization unit was deliberately set to a relatively low value of 5 dBm, packet rate to 100 packets per second, and channel 176 with a 10 MHz bandwidth was used. The ack transmit power was adjusted to 10 dBm and an omnidirectional antenna with a gain of 5 dBi was used. The null and the ack frame were BPSK modulated, with rate 1/2. Figure 6.1 shows the measurement results.

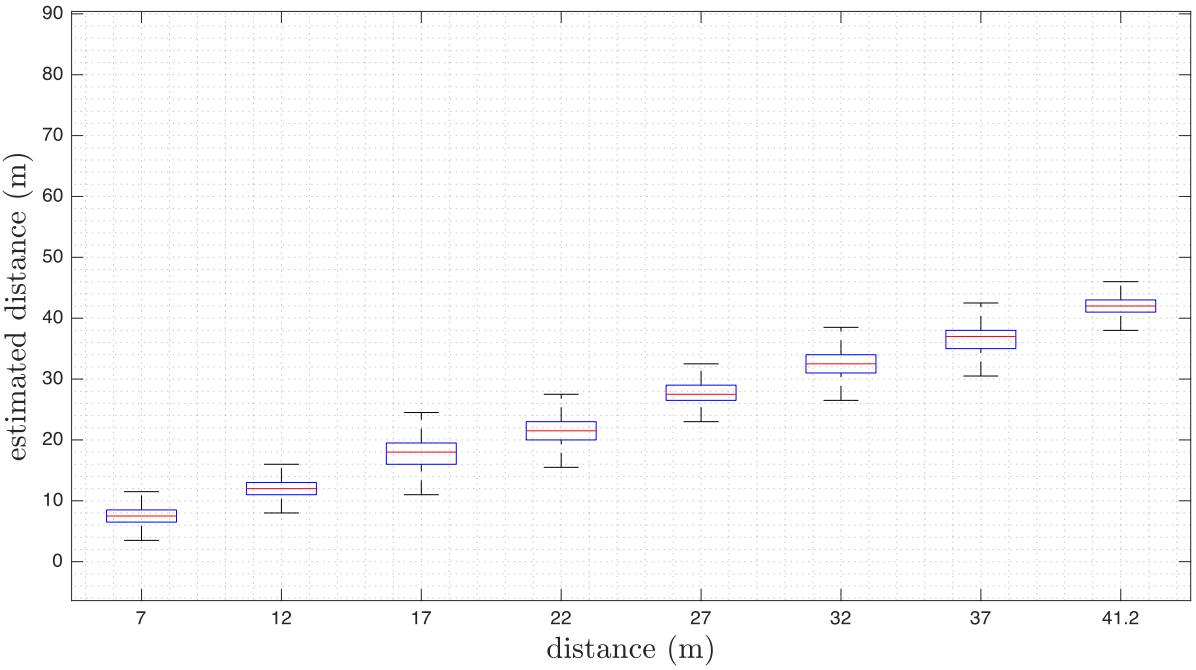

Figure 6.1: First outdoor measurement in Teesdorf; pseudorange estimation using two RSUs with omnidirectional antennas; the horizontal axis shows the actual distance; the vertical axis the estimated distance.

On the horizontal axis, the actual distance is shown. On the vertical axis, the estimated distance, calculated with (5.1). Here it is noticeable that the estimation error between the mean value and actual distance is at most 1 m (at 27 m). Repeating the measurements with slightly changed

parameters, such as transmit power, channel, packet rate, lead to the same result. Based on this series of measurements, we decided that an estimation using the ack frame is possible.

6.2 2D position estimation

The final position estimation application was tested in three measurement series. After each, the parameters and setup were tweaked and adjusted. The first test was done on the driving technique center in Teesdorf. The second two, at the Kapsch Components (KCO) parking space in Vienna.

6.2.1 Teesdorf measurements

The measurement setup can be seen in Figure 6.2a. Here, RSU_1 is mounted on a mobile trailer tower at a height of 6.2 m. The second RSU was directly mounted on the gentry at 7.8 m. In Figure 6.2b, the actual position of the RSUs can be seen. RSU_1 represents the origin of the reference coordinate system, RSU_2 is placed 10 m in positive x-direction and 8.5 m in the y-direction. The blue and orange line represent the boundary lines. Necessary for the coordinate transformation is the latitudinal and longitudinal position of RSU_1, which is (47.959 879, 16.280 066).

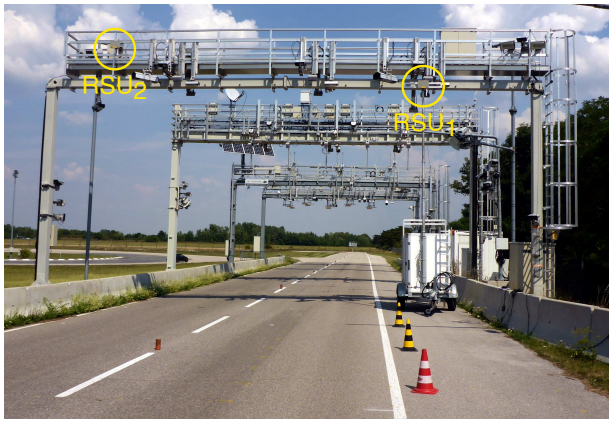

(a) Measurement setup; RSU_1 mounted on a mobile trailer tower at a height $h_1 = 6.2\,\text{m}$, RSU_2 mounted on the gantry at $h_2 = 7.8\,\text{m}$; both devices use omnidirectional antennas.

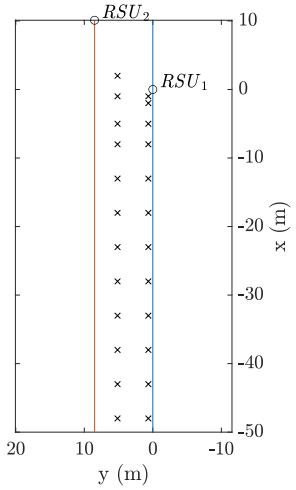

(b) Measurement points represented with an "x"; the orange and blue line represent the street boundaries, RSU_1 states the origin, RSU_2 is placed 10 m in positive x-direction and 8.5 m in the y-direction apart.

Figure 6.2: Outdoor test arrangement in Teesdorf

For the tests, the null frame transmit power was set to 20 dBm. Channel 178 with $BW = 10\,\text{MHz}$ and BPSK modulation scheme with code rate 1/2, was used. On both RSUs, omnidirectional

antennas with a gain of 6 dBi were installed. On the Kapsch CBX-9160 OBU, an omnidirectional broadband antenna with a gain of 5 dBi was mounted. The OBU software was not changed or adapted and was, therefore, in normal operation mode. In direct vicinity of the RSUs, the measurement points were placed in a smaller grid, 3 m apart, and after 8 m, the distance was increased to 5 m between consecutive points. For repeatability and reproducibility, the points were marked using pylons, placed along two lines parallel to the x-axis. One at $y = 5.15$ m, the other one at 0.65 m, as it can be seen in Figure 6.2b. The OBU was placed in the trunk of a minivan, the antenna was magnetically mounted on the left-middle of the roof. For the measurements, the car was placed at a pylon, and after starting the application, the OBU position was estimated within a one-second interval, for a time period of ~ 30 s. That means that at each point, ~ 30 estimations were obtained. In Figure 6.3, the results are shown. Here, the estimation error in the x- and y-direction (EE_x,EE_y) is calculated as:

$$\begin{aligned} EE_x &= x_{est} - x_{act} \\ EE_y &= y_{est} - y_{act} \end{aligned} \tag{6.1}$$

where x_{est},y_{est} is the estimated x- respectively y-coordinate and x_{act} and y_{act} the actual x- respectively y-position of the OBU.

The boxplot in Figure 6.3a shows the deviation in the x-direction, and Figure 6.3b shows the variation in the y-direction. What can be seen at first sight is that the variations compared to the one from Section 6.1 are significantly higher. The reason for that can be traced back to the way both RSUs were mounted. Figure 6.2a shows that directly behind the omnidirectional antenna from RSU_1, is a steel beam and behind RSU_2 is an aluminum shield, causing multipath fading. However, it turned out, that the sheet metal roof of the car on which the antenna of the OBU was mounted, did not have an influence. It is also noticeable that with increasing distance between the OBU and the RSUs, the estimation error (see Figure 6.3(a),(b)) increases as well. This behavior is due to the RSU position and the measurement corridor. Assuming that the RSU positions relative to each other are compared to the distance between RSU and OBU, small, the problem of glancing intersection appears. Figure 6.4 illustrates the issue. The RSUs are positioned as in the measurement setup, the OBU is located at $(-40, 0)$. The black dotted arc corresponds to the error-free estimation, the red dotted segment of a circle to the erroneous estimation. Here, RSU_1 estimates the pseudorange to be one meter longer, RSU_2 estimates it to be one meter shorter. This two meter difference results in a y-direction shift of 10.4 m and an x-direction shift of 0.4 m. Compared to the multipath problem, this issue can be solved rather easily by redefining the measurement corridor and changing the RSU positions.

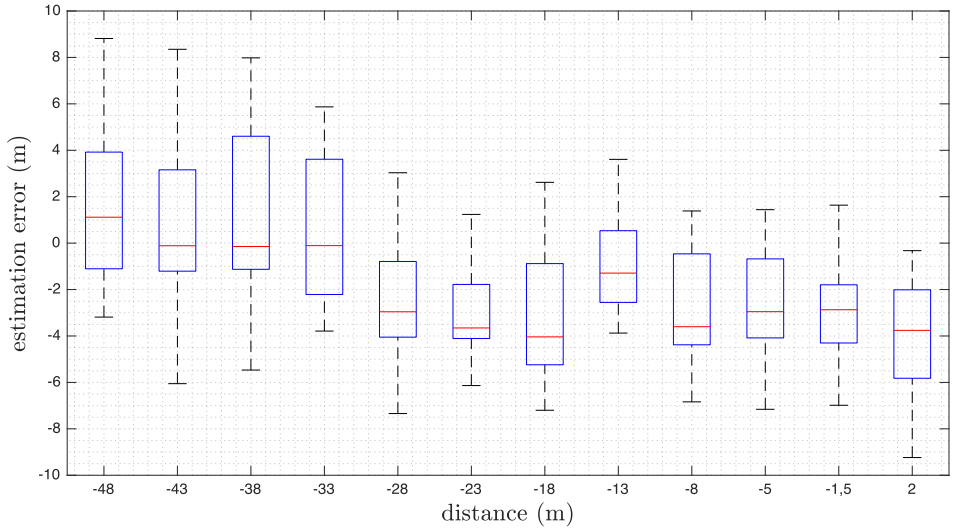

(a) Position estimation error along the road; the vertical axis shows the estimation error in regards to the x-direction.

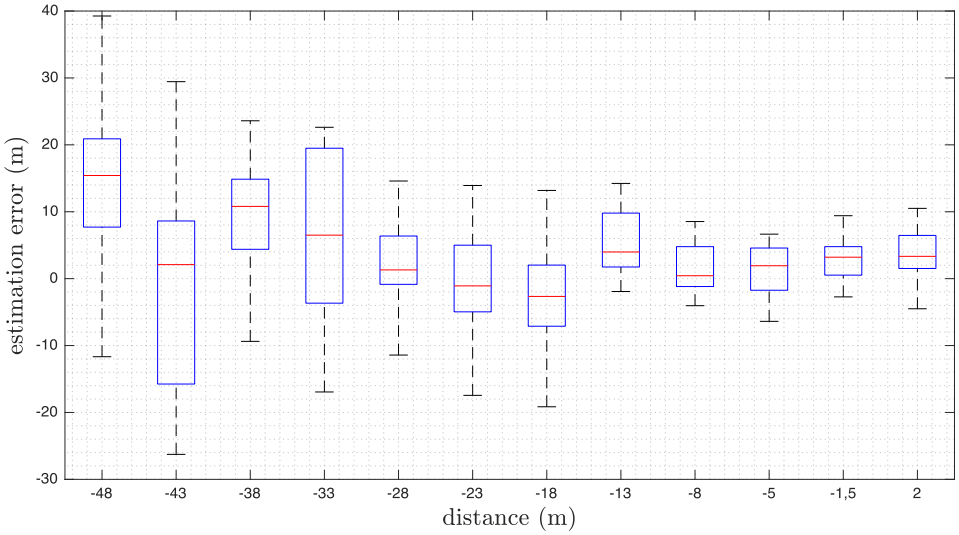

(b) Position estimation error in lateral direction; the vertical axis shows the estimation error in regards to the y-direction.

Figure 6.3: Boxplot of the estimation accuracy using omnidirectional antennas; OBU is placed at $y = 5.15\,\text{m}$ and moved along the x-direction. The horizontal axis shows the distance from RSU_1 to OBU. At each position, ~ 30 estimations were taken.

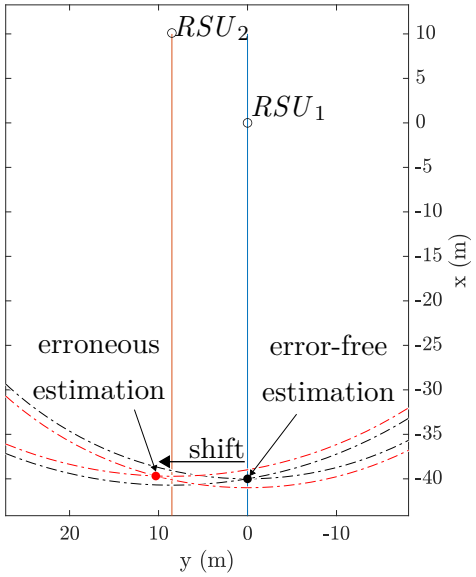

Figure 6.4: Problem of glancing intersection at larger distances between RSU and OBU. Red dot shows the erroneous estimation, black dot the error-free estimation. An assumed error in the pseudorange of two meters results in a 10.5 m deviation in lateral direction.

6.2.2 KCO measurements I

After the measurement series in Teesdorf, we measured a second time, with the same transmission parameters as used in Section 6.2.1, at the Kapsch Components factory's parking space in Vienna. An optimized RSU position setup, minimizing the problem of a glancing intersection was calculated, the position of the RSUs were changed accordingly and the measurement corridor redefined. Two setups turned out to be equally good. One, where the two RSUs are placed along a line, on the same side of the road, cf. Figure 6.5b, and another one, where the second RSU is placed diagonally, as it can be seen in Figure 6.5c. The second problem which was noticed at the Teesdorf measurement was the susceptibility to multipath fading. To solve that problem, we improved the mounting of the RSU. As seen in Figure 6.5a, RSU_1 was mounted on an aluminum stand, which has as little as possible reflecting surface exposed to the electromagnetic signal radiated from the device. The second RSU was put on an office chair with a plastic backrest. To further reduce multipath effects, in addition to the omnidirectional antennas with 6 dBi gain, linear polarized directional antennas with a gain of 14 dBi were tested. A sidelobe suppression of 15 dB should minimize destructive superposition. The OBU was placed in a rolling cart and pushed along a predefined line, parallel to the x-axis, at a distance $y = 2\,\text{m}$. Transmission parameters stayed unchanged. At each point, ~ 30 position estimations were taken. On the boxplots in Figure 6.6, the results for the inline positioned RSUs can be seen. The plot on the top, Figure 6.6a, shows the estimation error in the x-direction, measured with the directional antenna, in the plot abbreviated as "Dir.", and the omnidirectional antenna, abbreviated as

"Omn.". The estimation error was calculated using (6.1). It can be seen, that both antennas perform nearly equally well. Although the mean value is not far off the actual distance, the variances are still higher than expected. Interestingly, the influence of a parked car at $x \approx 20\,\text{m}$ is noticeable. Here, the variance is drastically bigger. In Figure 6.6b, the estimation error in the y-direction is shown. The influence of the car is also perceivable. Compared to the results obtained from the Teesdorf measurements, it can be seen that the overall estimation accuracy has increased and is not distance-dependent any more. In addition to that, the second solution can be easily filtered since it violates the boundary conditions.

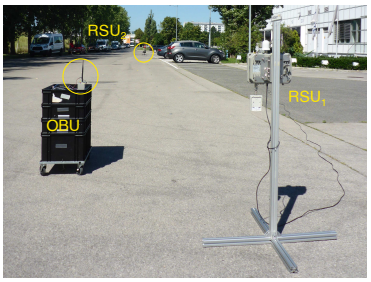

(a) Measurement setup; RSU_1 mounted on an aluminium stand to reduce signal reflections, RSU_2 stands on an office chair; OBU is placed in a rolling cart

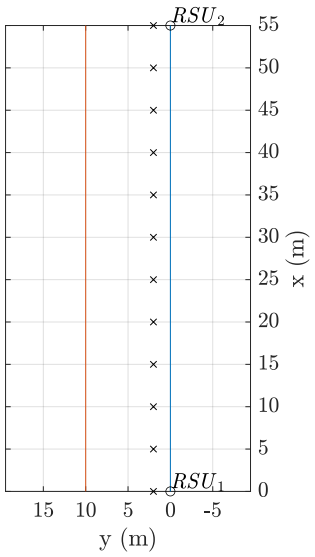

(b) Inline setup; RSU_2 is placed 55 m in positive x-direction, inline with RSU_1

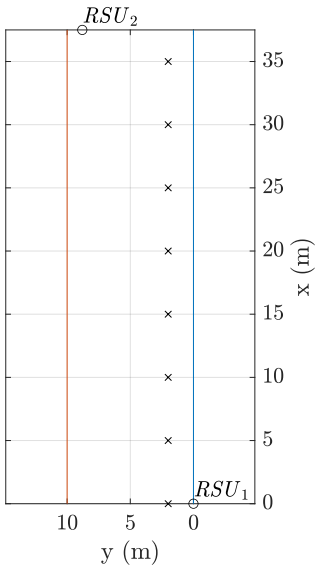

(c) Diagonal setup;RSU_2 is placed $x = 40\,\text{m}$ and and $y = 9\,\text{m}$

Figure 6.5: KCO I measurement setup; localization corridor is in between the RSUs; RSU_1 states the origin $(0, 0)$; measurement points represented with a "x"; the orange and blue line represent the street boundaries.

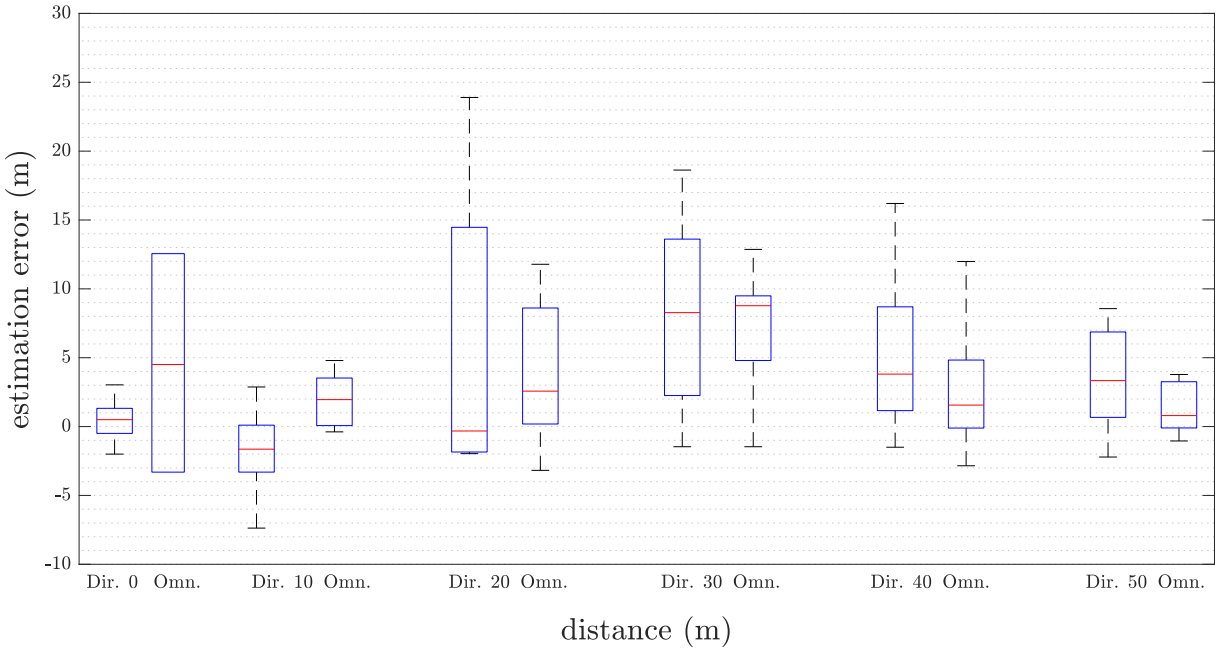

(a) Position estimation error along the road; the vertical axis shows the estimation error in regards to the x-direction.

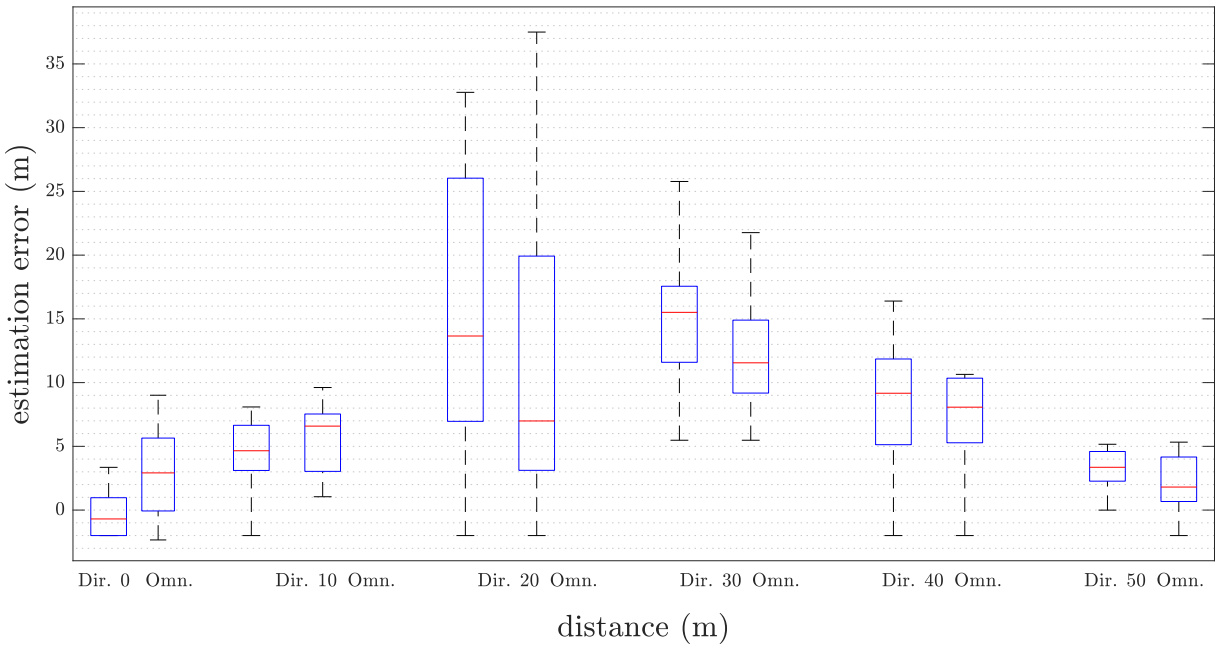

(b) Position estimation error in lateral direction; the vertical axis shows the estimation error in regards to the y-direction.

Figure 6.6: Position estimation measurements using a directional "Dir." and an omnidirectional antenna "Omn."; RSUs placed along a line; OBU is placed at $y = 2\,\mathrm{m}$ and moved along the x-direction. The horizontal axis of the boxplot shows the distance from RSU_1 to OBU. At each position, ~ 30 estimations were taken.

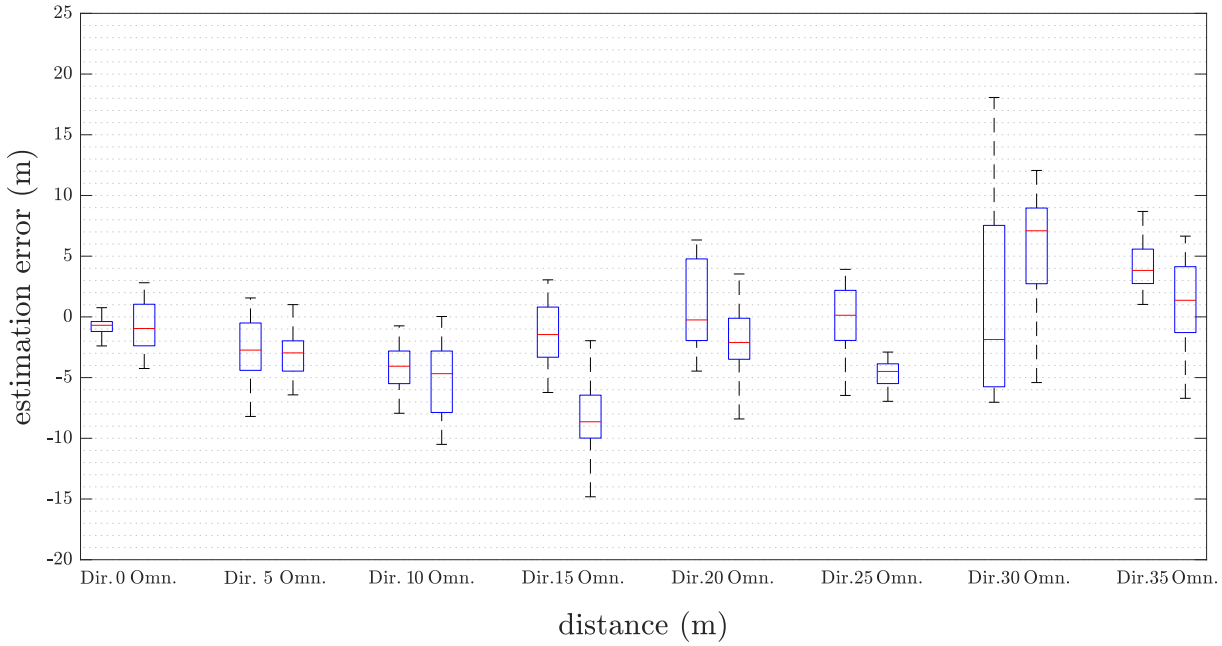

(a) Position estimation error along the road; the vertical axis shows the estimation error in regards to the x-direction.

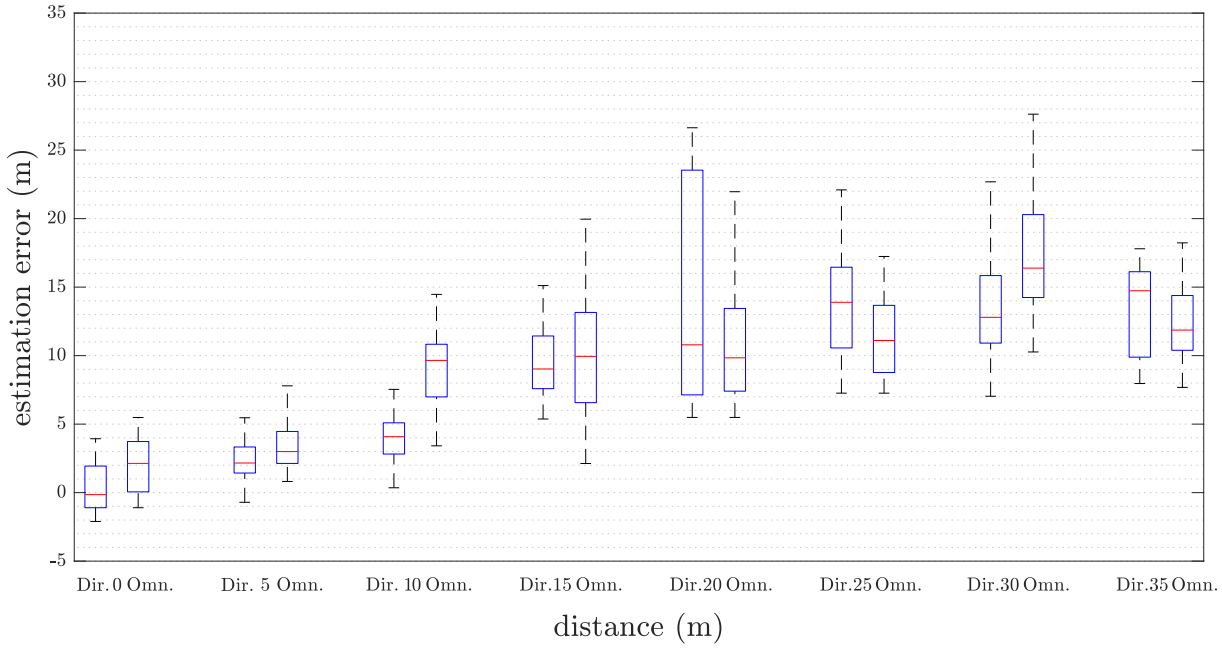

(b) Position estimation error in lateral direction; the vertical axis shows the estimation error in regards to the y-direction.

Figure 6.7: Boxplot of the position estimation measurements using a directional "Dir." and an omnidirectional antenna "Omn."; RSUs placed diagonally; OBU is placed at $y = 2\,\text{m}$ and moved along the x-direction. The horizontal axis shows the distance from RSU_1 to OBU. At each position, ~ 30 estimations were taken.

In Figure 6.7, the measurement results, with the RSUs positioned diagonally, are shown. We measured twice, once with the omnidirectional antenna, the other time with directional antennas. Apart from the RSU position, the settings remained unchanged. In Figure 6.7a, the estimation error in the x-direction can be seen. The results are comparable to the previous ones (see Figure 6.6a). The differences between the omnidirectional and directional antenna regarding variances are negligible.
It can be seen that the error in lateral direction increases with distance. This may be due to the parked car, but it could not be verified. However, the setup with the RSUs placed along a line is preferable since the second, unwanted solution can be easily detected and filtered out.

6.2.3 KCO measurements II

Since the last measurements had shown that the estimation error is still unsatisfying, one final attempt was started to increase accuracy. The transmission parameters remained as in Section 6.2.1.
Small-scale fading occurs in the range of a half wavelength, which equals $\sim 3\,\text{cm}$. Because the V2X measurement environment constantly changes, averaging over two consecutive measurements could increase performance. Instead of a single RTT, the average of two consecutive measurements is sent to the MEU. The time between the two measurements was set to be $100\,\mu\text{s}$. The following only shows the results taken with the omnidirectional antennas, since difference between them and the directional antennas was neglectable. In Figure 6.8a, the estimation error in x-direction is shown. Here, we can see that the variance is significantly smaller, and the overall estimation error was reduced. However, looking at Figure 6.8b, the results are similar to the previous ones.
It is also noteworthy that the influence of the car, which was this time parked at $x \approx 30\,\text{m}$, is still not reduced. Furthermore, averaging two RTT measurements also means that if one of the two is an outlier, the averaged value is still off. However, with the given hardware and the limited information extractable from the radio module, this was the solution which achieved the best position estimation accuracy.

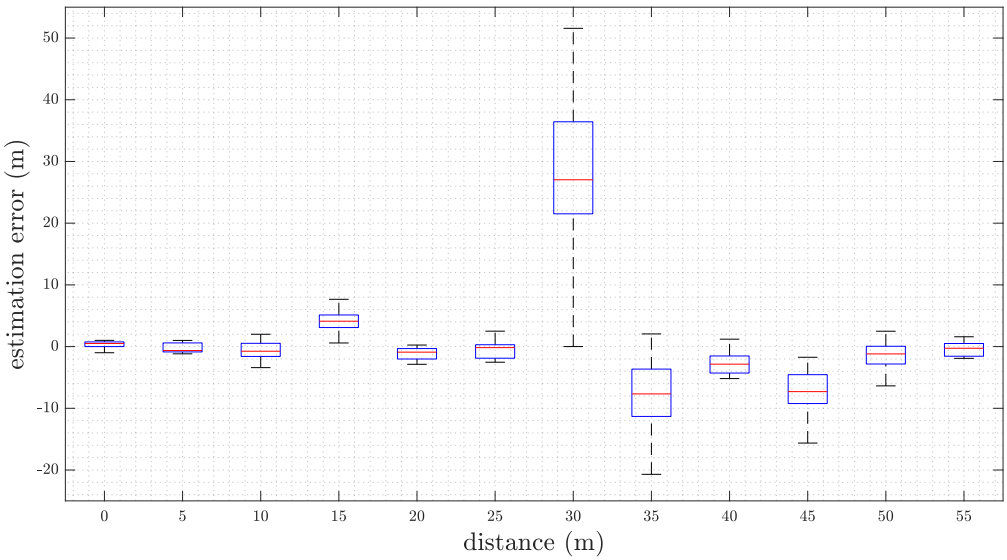

(a) Position estimation error along the road; the vertical axis shows the estimation error in regards to the x-direction.

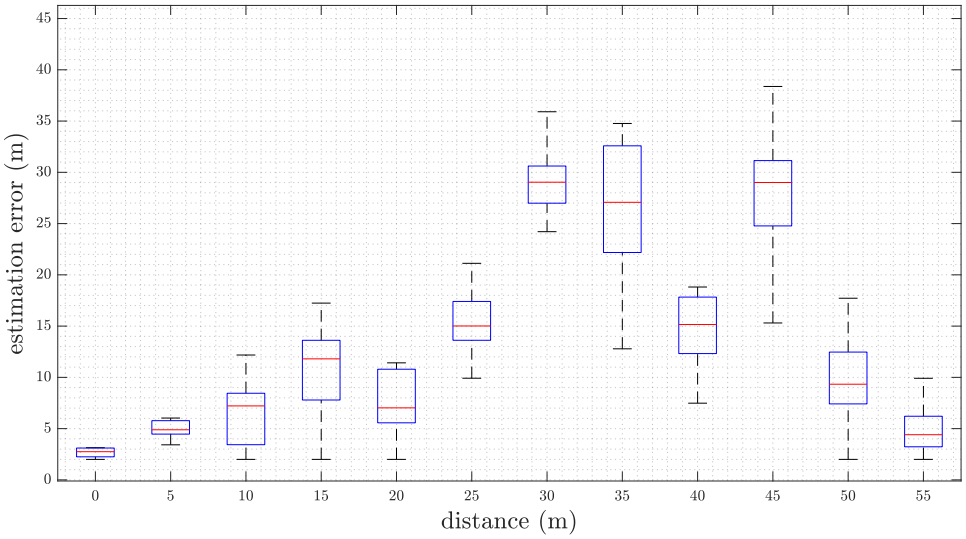

(b) Position estimation error in lateral direction; the vertical axis shows the estimation error in regards to the y-direction.

Figure 6.8: KCO II measurement series; improved application with two consecutive RTT measurements; RSUs placed along a line; OBU is placed at $y = 2\,\mathrm{m}$ and moved along the x-direction. The horizontal axis shows the distance from RSU_1 to OBU. At each position, ~ 30 estimations were taken using an omnidirectional antenna.

For the final measurement, the two RSUs, equipped with omnidirectional antennas, were placed 55 m apart, along a line. The OBU was put in the rolling cart and moved with a speed of $\sim 1\,\mathrm{m\,s^{-1}}$ from RSU_2 towards RSU_1 and back along the red line, as shown in Figure 6.9. Only

the east boundary was used (blue line). The estimations were smoothed using the implemented moving average filter with a span of eight samples. As it can be seen, the parked car, marked with a yellow circle, has a significant impact on the estimation accuracy. Further filtering or estimation algorithms would not increase accuracy since the measurement values vary too much, and additional readings like the RSSI are not available. However, the application can be operated in a slimmed-down mode, in which the position along the road is estimated only and the OBU is effectively positioned in the middle of the road. Therefore, the boundary conditions have to be set to match the road width.

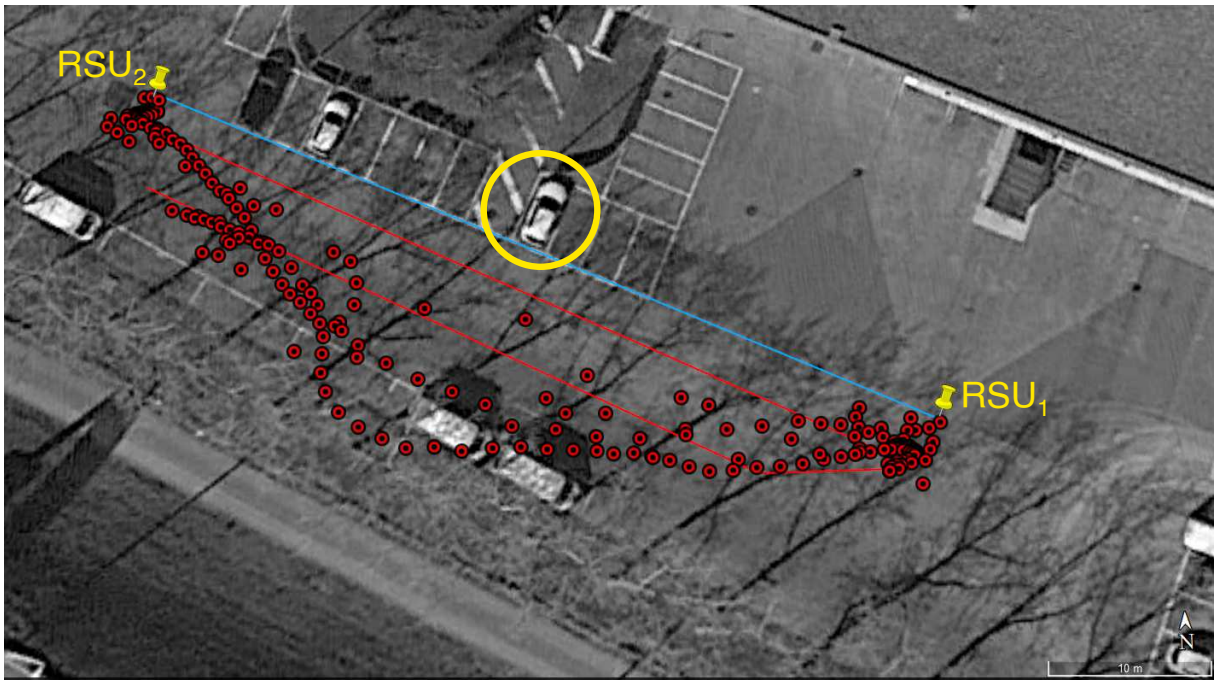

Figure 6.9: Smoothed position estimation using omnidirectional antennas; RSUs are placed 55 m apart; influence of the parked car can be seen.

7

Conclusion

An easy to deploy position estimation application for the use in V2X systems was proposed, analyzed, prototypically implemented and validated by measurements. Hereby, the localization is done via the RTT readings of the acknowledgment frame used in IEEE 802.11. First, the Kapsch RSU radio's behavior was analyzed to decide whether the proposed method could work. Therefore, over 90 measurement series and tests have been conducted to determine the radio module's behavior, depending on various influences. Among others, the dependency on temperature, modulation type, code rate, correlation between the RTT and the transmit power, as well as the effect of multipath propagation, was measured.

The radio module's behavior was modeled in MATLAB together with potential deployment challenges. A digital twin of the application was implemented in MATLAB. Various scenarios were implemented to simulate key scenarios to minimize costly and time-consuming measurement campaigns. That included adjustable timing offsets, variable distributions emulating real-world behavior of the RTT, and configurable RSU geometries. Since the application's code had to be implemented in C language, care was taken to formulate the algorithms robustly.

The next step was to implement the used algorithms into the ITS-G5 stack, deployed at the RSUs. It was essential to keep the impact of the localization application as small as possible since the main functionality should not be disturbed. Further, the use of unicast messages in V2X systems is not foreseen in ITS-G5 and, hence, not implemented by default. Therefore, I needed to do this in my work which meant modifying the stack's access layer. To keep the system modular and thereby avoiding synchronization among the RSUs, a method was developed where the RSUs can simultaneously send localization frames to the OBU. It is also possible to add additional RSUs to the localization process without changing the code on the RSU side.

An evaluation unit was implemented, deployable either on an RSU or any other Linux based device. The data exchange is done via a UDP connection.

The implementation was tested outdoors in three measurement campaigns during summer 2020. Different RSU positions, antenna setups, and transmission parameters were configured for measurement scenarios. After each measurement series, the software implementation was further improved.

As it turned out, multipath fading has a significant impact on accuracy. If only two RSUs are deployed, the multipath effects can neither be suppressed nor filtered out. However, the application can be operated in a slimmed-down mode, in which the position along the road is estimated only. In this case, the position estimate in lateral direction is not evaluated, and the OBU is effectively positioned in the middle of the road.

With the available hardware, the position estimate of an OBU is unreliable if based on RTT values only. Combining the RTT with RSS readings has the potential to significantly improve the results. Moreover, using three or more RSUs for the process enables detecting erroneous readings and filter them out. It also allows determining the direction of travel. The application itself, the quasi-simultaneous transmission of null frames without synchronization, worked as expected and is usable for later developments.

Bibliography

[1] *5GAA: ITS spectrum*. visited on 26-03-2020. URL: https://5gaa.org/wp-content/uploads/2018/07/5GAA_WhitePaper_ITS-spectrum-utilization-in-the-Asia-Pacific-Region_FINAL_160718docx.pdf.

[2] Abdeldime MS Abdelgader and Wu Lenan. "The physical layer of the IEEE 802.11 p WAVE communication standard: the specifications and challenges". In: *Proceedings of the world congress on engineering and computer science*. Vol. 2. 2014, pp. 22–24.

[3] Labyad Asmaa, Kharraz Aroussi Hatim, and Mouloudi Abdelaaziz. "Localization algorithms research in wireless sensor network based on Multilateration and Trilateration techniques". In: *2014 third IEEE international colloquium in information science and technology (CIST)*. IEEE. 2014, pp. 415–419.

[4] *C2C:C-ITS*. visited on 24-03-2020. URL: https://www.car-2-car.org/.

[5] *Capital: ITS*. visited on 23-03-2020. URL: https://www.its-elearning.eu/courses.

[6] Marc Ciurana, Francisco Barcelo-Arroyo, and Fernán Izquierdo. "A ranging method with IEEE 802.11 data frames for indoor localization". In: *2007 IEEE Wireless Communications and Networking Conference*. IEEE. 2007, pp. 2092–2096.

[7] RH Clarke. "A statistical theory of mobile-radio reception". In: *Bell system technical journal* 47.6 (1968), pp. 957–1000.

[8] *DOT: DSRC report*. visited on 26-03-2020. URL: https://www.its.dot.gov/research_archives/connected_vehicle/pdf/DSRCReportCongress_FINAL_23NOV2015.pdf.

[9] EN ETSI. "302 665". In: *Intelligent transport systems (ITS)* (2010), pp. 1–44.

[10] TCITS ETSI. "European profile standard for the physical and medium access control layer of Intelligent Transport Systems operating in the 5 GHz frequency band". In: *ETSI ES* 202 (2009), p. 663.

[11] *ETSI: ITS-G5*. visited on 26-03-2020. URL: https://www.etsi.org/deliver/etsi_en/302600_302699/302663/01.03.00_20/en_302663v010300a.pdf.

[12] *EU Directive 2010/40/EU*. visited on 27-03-2020. URL: https://eur-lex.europa.eu/legal-content/EN/TXT/HTML/?uri=LEGISSUM:tr0040&from=EN.

[13] Reinhard Exel. "Time-Based Radio Localization in IEEE 802.11b Wireless Local Area Networks". PhD thesis. Technische Universität Wien, 2012.

[14] Alessio Fascista et al. "A localization algorithm based on V2I communications and AOA estimation". In: *IEEE Signal Processing Letters* 24.1 (2016), pp. 126–130.

[15] Harald T Friis. "A note on a simple transmission formula". In: *Proceedings of the IRE* 34.5 (1946), pp. 254–256.

[16] Matthew S Gast. *802.11 Wireless Networks: The Definitive Guide, Second Edition*. O'Reilly Media, Inc., 2005. ISBN: 0596100523.

[17] Andrea Goldsmith. *Wireless communications*. Cambridge university press, 2005.

[18] Ali Grami. *Introduction to Digital Communications*. Academic Press, 2015.

[19] IEEE 802.11 Working Group et al. "Part 11: Wireless LAN Medium Access Control (MAC) and Physical Layer (PHY) specifications". In: *IEEE Std 802.11* (2016).

[20] Satish R Jondhale and Rajkumar S Deshpande. "Kalman filtering framework-based real time target tracking in wireless sensor networks using generalized regression neural networks". In: *IEEE Sensors Journal* 19.1 (2018), pp. 224–233.

[21] Yunxin Jeff Li. "An overview of the DSRC/WAVE technology". In: *International Conference on Heterogeneous Networking for Quality, Reliability, Security and Robustness*. Springer. 2010, pp. 544–558.

[22] Ivan A Mantilla-Gaviria et al. "Localization algorithms for multilateration (MLAT) systems in airport surface surveillance". In: *Signal, Image and Video Processing* 9.7 (2015), pp. 1549–1558.

[23] Guoqiang Mao, Bar Fidan, and Brian DO Anderson. "Wireless sensor network localization techniques". In: *Computer networks* 51.10 (2007), pp. 2529–2553.

[24] Gerald Matz. *Lecture notes: Wireless OFDM systems*. Sept. 2019.

[25] Dennis D McCrady et al. "Mobile ranging using low-accuracy clocks". In: *IEEE Transactions on Microwave Theory and Techniques* 48.6 (2000), pp. 951–958.

[26] Andreas F Molisch. *Wireless communications*. Vol. 34. John Wiley & Sons, 2012.

[27] José A del Peral-Rosado et al. "Feasibility study of 5G-based localization for assisted driving". In: *2016 International Conference on Localization and GNSS (ICL-GNSS)*. IEEE. 2016, pp. 1–6.

[28] *Publications Office of the EU: ITS Support Study*. visited on 27-03-2020. URL: `https://op.europa.eu/s/n2go`.

[29] Theodore S Rappaport et al. *Wireless communications: principles and practice*. Vol. 2. prentice hall PTR New Jersey, 1996.

[30] Steven O Rice. "Statistical properties of a sine wave plus random noise". In: *The Bell System Technical Journal* 27.1 (1948), pp. 109–157.

[31] Yuvraj Singh. "Comparison of okumura, hata and cost-231 models on the basis of path loss and signal strength". In: *International journal of computer applications* 59.11 (2012).

[32] Warren L Stutzman and Gary A Thiele. *Antenna theory and design*. John Wiley & Sons, 2012.

[33] Han-Shue Tan and Jihua Huang. "DGPS-based vehicle-to-vehicle cooperative collision warning: Engineering feasibility viewpoints". In: *IEEE Transactions on Intelligent Transportation Systems* 7.4 (2006), pp. 415–428.

[34] Peter Teunissen and Oliver Montenbruck. *Springer handbook of global navigation satellite systems*. Springer, 2017.

[35] F-Y Wang, Charles Herget, and Daniel Zeng. "Guest editorial developing and improving transportation systems: the structure and operation of IEEE intelligent transportation systems society". In: *IEEE Transactions on Intelligent Transportation Systems* 6.3 (2005), pp. 261–264.

[36] Anthony J Weiss. "Direct position determination of narrowband radio frequency transmitters". In: *IEEE signal processing letters* 11.5 (2004), pp. 513–516.

[37] Zheng Yang and Yunhao Liu. "Quality of trilateration: Confidence-based iterative localization". In: *IEEE Transactions on parallel and distributed systems* 21.5 (2009), pp. 631–640.

Hiermit erkläre ich, dass die vorliegende Arbeit gemäß dem Code of Conduct, insbesondere ohne unzulässige Hilfe Dritter und ohne Benutzung anderer als der angegebenen Hilfsmittel, angefertigt wurde. Die aus anderen Quellen direkt oder indirektübernommenen Daten und Konzepte sind unter Angabe der Quelle gekennzeichnet. Die Arbeit wurde bisher weder im In noch im Ausland in gleicher oder in ähnlicher Form in anderen Prüfungsverfahren vorgelegt.

Wien, November 2020 Richard Pfister